The effect of ocean ventilation on the Transient Climate Response to Emissions

Anna Katavouta * and Richard G. Williams

Department of Earth Ocean and Ecological Sciences, School of Environmental Sciences, University of Liverpool, Liverpool, UK

Philip Goodwin

School of Ocean and Earth Sciences, University of Southampton, Southampton, UK

**Corresponding author address:* Anna Katavouta, Department of Earth Ocean and Ecological Sciences, University of Liverpool, Liverpool, UK

E-mail: a.katavouta@liverpool.ac.uk

ABSTRACT

The surface warming response to carbon emissions is affected by how the ocean sequesters excess heat and carbon supplied to the climate system. This ocean uptake involves the ventilation mechanism, where heat and carbon are taken up by the mixed layer and transferred to the thermocline and deep ocean. The effect of ocean ventilation on the surface warming response to carbon emissions is explored using simplified conceptual models of the atmosphere-ocean with and without explicit representation of the meridional overturning. Sensitivity experiments are conducted to investigate the effects of (i) mixed-layer thickness, (ii) rate of ventilation of the ocean interior, (iii) strength of the meridional overturning and (iv) extent of subduction in the Southern Ocean. Our diagnostics focus on a climate metric, the Transient Climate Response to carbon Emissions (TCRE), defined by the ratio of surface warming to the cumulative carbon emissions, which may be expressed in terms of separate thermal and carbon contributions. The variability in the thermal contribution due to changes in ocean ventilation dominates the variability in the TCRE on timescales of years to centuries, while that of the carbon contribution dominates on timescales of several centuries to millennia. These ventilated controls are primarily from changes in the mixed-layer thickness on decadal timescales, and in the rate of ventilated transfer from the mixed layer to the thermocline and deep ocean on centennial and millennial timescales, which is itself affected by the strength of the meridional overturning and extent of subduction in the Southern Ocean.

1. Introduction

Climate model projections reveal that the global-mean surface warming increases nearly linearly with cumulative carbon emissions (Allen et al. 2009; Gillet et al. 2013; Matthews et al. 2009; Zickfeld et al. 2009). This proportionality between the global-mean increase in surface air temperature and the cumulative carbon emissions has been used to define a climate metric in Earth system models, referred to as the Transient Climate response to cumulative carbon Emissions (TCRE).

The ocean plays a central role in determining this connection between surface warming and carbon emissions through ocean uptake of heat and carbon (Solomon et al. 2009). The ocean uptake of atmospheric CO_2 acts to decrease radiative forcing and so provides a cooling effect, while the proportion of radiative forcing driving ocean heat uptake declines in time and so provides a warming effect (Goodwin et al. 2015; Williams et al. 2016, 2017a).

The dependence of surface warming on carbon emissions differs in magnitude between different models, such as with the TCRE varying between 1.20 and 2.45 K $(1000\ \mathrm{PgC})^{-1}$ in a suite of 10 CMIP5 models with an annual 1% rise in atmospheric CO_2 (Williams et al. 2017b). Their inter-model differences in the TCRE arise mostly from differences in the thermal response on decadal to multi-decadal timescales, with differences in the carbon response becoming important on multi-decadal to centennial timescales (Williams et al. 2017b). The inter-model spread in climate feedbacks (Andrews et al. 2012; Forster et al. 2013) is the largest driver of uncertainty in the TCRE, but the inter-model spread in ocean heat uptake also contributes (Raper et al. 2002; Geoffroy et al. 2012; MacDougall et al. 2017; Williams et al. 2017b). What is unclear is the effect of different ocean ventilation mechanisms in controlling this surface warming dependence on carbon emissions and in leading to inter-model differences in the TCRE.

The ocean uptake of anthropogenic heat and carbon is primarily controlled by the ventilation process involving uptake of heat and carbon by the surface mixed layer and subsequent transfer into the main thermocline and the deep ocean. This ventilated response is affected by the strength of the Atlantic meridional overturning circulation, which in turn alters the surface warming response to carbon emissions (Xie and Vallis 2012; Rugenstein et al. 2013; Winton et al. 2013). The Atlantic meridional overturning circulation varies significantly amongst Earth system models (Gregory et al. 2005; Cheng et al. 2013) and this variation is partially responsible for the spread in the transient warming due to emissions (Kostov et al. 2014). However, ocean ventilation is not solely controlled by the strength of the meridional overturning circulation, but also affected by the thickness of the mixed layer, and the horizontal gyre, eddy and circumpolar circulations affecting the formation of mode waters and their spreading into the thermocline and ocean interior. Hence, we need to understand how the full range of physical effects contributing to ocean ventilation help determine the climate response of a model.

In this study we investigate how the climate metric, the Transient Climate Response to cumulative carbon Emissions, is controlled by: (i) the thickness of the mixed layer in contact with the atmosphere; (ii) the rate of ventilation between the mixed layer and the ocean interior; (iii) the strength of the meridional overturning; and (iv) the extent of Southern Ocean mode water formation. To address these questions, we take a step back from the complex Earth system models and conduct sensitivity experiment using idealised atmosphere-ocean models, so as to provide a clearer mechanistic connection between the effects of different processes contributing to ventilation and the TCRE. Since observational reconstructions reveal enhanced uptake of anthropogenic heat and carbon in the upper thermocline over the global ocean (Sabine et al. 2004; Roemmich et al. 2015), one of our conceptual models include a thermocline with a dynamically-controlled thickness (Gnanadesikan 1999; Marshall and Zanna 2014).

The outline of the paper is as follows. The formulation of the idealised models and sensitivity experiments are first presented (Section 2). The climate response in the sensitivity experiments is interpreted by separating the dependence of surface warming on carbon emissions, as given by the TCRE, into a product of thermal and carbon contributions (Williams et al. 2016) and identifying the relative importance of the different processes contributing to ocean ventilation (Section 3). The effect of different ventilation processes on the TCRE is assessed across parameter space by diagnosing the response of a large set of model ensembles (Section 4). Finally, the implications and the caveats to the study are discussed (Section 5).

2. Model formulation and experiments

The effect of different processes contributing to ocean ventilation on the climate metric, the TCRE, are investigated using two idealised box models of the atmosphere-ocean system, either without or with an explicit representation of the ocean meridional overturning circulation.

a. 1D box model of the atmosphere-ocean

The 1D box model consists of three homogeneous layers: a slab atmosphere, an ocean mixed layer and an ocean interior (Fig.1a). The model solves for the heat and carbon exchange due to carbon emissions between these layers, including physical and chemical transfers, but ignoring biological transfers, and sediment and weathering interactions; see supplementary material in Katavouta et al. (2018). Ocean ventilation is represented by the ocean interior taking up the temperature and carbon anomalies of the mixed layer with a relaxation closure, such that the rates of change in the temperature and the dissolved inorganic carbon of the ocean interior are described by

$$\frac{d}{dt}T_{int}(t) = \frac{1}{\tau_{vent}}\left(\Delta T_{ml}(t) - \Delta T_{int}(t)\right), \tag{1a}$$

$$\frac{d}{dt}DIC_{int}(t) = \frac{1}{\tau_{vent}}\left(\Delta DIC_{ml}(t) - \Delta DIC_{int}(t)\right), \tag{1b}$$

where τ_{vent} is a relaxation timescale referred to as the ventilation timescale, $\Delta T(t)$ is the temperature change in K and $\Delta DIC(t)$ the carbon change in mol kg^{-1} relative to the pre-industrial, and subscripts *ml* and *int* refer to the ocean mixed layer and interior values; this model is referred to as the 1D box model.

b. Box model of the atmosphere-ocean with meridional overturning

Our box model of the atmosphere and ocean with meridional overturning (Fig.1b) follows the layered model of the global thermocline by Gnanadesikan (1999) and the extensions by Johnson et al. (2007) and Marshall and Zanna (2014).

Light water is transformed to dense water by surface cooling in the northern high latitudes, at a volume rate of q_{NA}, equivalent to the strength of the meridional overturning. Dense water is transformed back to light water either by diapycnal transfers in the low latitudes, at a volume rate of q_v, or by a surface warming conversion into light waters in the southern high latitudes associated with the residual circulation, at a volume rate of q_{so}, involving a northward Ekman volume flux partly compensated by a poleward mesoscale eddy flux. The volume of light waters and overturning strength, q_{NA}, is then controlled in a dynamic manner in terms of the diapycnal mixing parametrised by a diapycnal mixing coefficient, the wind stress in the Southern Ocean, the strength of the eddies in the Southern Ocean parametrised by the eddy diffusivity, and the additional ocean warming and enhancement of stratification due to the anthropogenic emissions (see Appendix for the closures).

To define the extent of ventilation, the light waters in the low latitudes extend over a variable thickness, $h(t)$, which are further separated into two layers: a mixed layer with constant thickness, $h_{ml} = 100$ m, and a thermocline layer with thickness, $h_{therm}(t) = h(t) - h_{ml}$ (Fig.1b).

To take into account the extent of communication between the atmosphere and the upper ocean, an isolation fraction, δ, is defined. This isolation fraction δ defines the relative proportion of the subduction occurring in the Southern Ocean and sets the fraction of waters remaining below the mixed layer and spreading northward within the thermocline; instead $(1-\delta)$ sets how much of the subduction occurs in the low latitudes and the fraction of waters in contact with the atmosphere in the tropics and subtropics. A rough estimate of δ corresponds to the ratio of the volume of waters subducted in the southern high latitudes, consisting of Sub-Antarctic mode water and Antarctic Intermediated Water, and transported northward versus the total volume of waters subducted and transported northward to the northern high latitudes, consisting of subtropical mode water, Sub-Antarctic mode water and Antarctic Intermediate Water. Based on the water-mass diagnostics of Talley (1999) at 24^{o}N, this partitioning implies that the ratio δ is about 0.7, suggesting that most of the subducted waters are from the Southern Ocean and so these waters are shielded from the atmosphere in the low latitudes.

A slab atmosphere is used to parametrise the exchange of heat and carbon between the atmosphere and the ocean, and two upper ocean boxes are used to represent the southern and northern high latitudes. These high latitude boxes are used to solve for the heat and carbon transfer in the ocean, but do not directly affect the model dynamics and volume transports (see Appendix for model closures). The model solves for the ocean carbon cycle including physical and chemical transfers, but ignores biological transfers, and sediment and weathering interactions involving changes in the cycling of organic carbon or calcium carbonate. The ocean carbonate system is solved using the iterative algorithm of Follows et al. (2006) and assumes that the total alkalinity remains constant: the model solves for the changes in pH and the fraction of carbonate species present in seawater and its effect on the the capacity of the ocean to absorb the changes in atmospheric CO_2. This idealised model is referred to as the box model with overturning.

c. Sensitivity experiments

The climate response is explored in both box models to carbon emissions, emitted to the atmosphere at a constant rate of 20 PgC y^{-1} for 100 years, and then integrated until equilibrium is reached after several 1000 years. The resulting increase in atmospheric CO_2 drives a radiative forcing: $R(t) = a\Delta \ln CO_2(t)$ (Myhre et al. 1998), where $a = 5.35$ W m^{-2} and the pre-industrial $CO_2(t_o)$ is 280 ppm. This radiative forcing, $R(t)$, is assumed to drive a global-mean radiative response, $\lambda(t)\Delta T(t)$, plus a planetary heat uptake, $N(t)$, (Gregory et al. 2004; Gregory and Forster 2008), such that

$$R(t) = \lambda(t)\Delta T(t) + N(t), \tag{2}$$

where $\lambda(t)$ is the climate feedback parameter, which is assumed constant and equal to 1 W $m^{-2}K^{-1}$ in all our simulations for simplicity. This λ value is close to the CMIP5 Earth system models mean of 1.13 W $m^{-2}K^{-1}$ (Forster et al. 2013). The planetary heat uptake, $N(t)$, is dominated by the ocean heat uptake (Church et al. 2011), and in both models, more than 95% of heat passes into the ocean; henceforth, the planetary and the ocean heat uptakes are taken to be effectively equivalent. The ocean carbon and heat uptakes due to the anthropogenic carbon emissions are approximated to be spatially uniform in these simplified conceptual models.

The 1D box model is used to explore the climate response and the sensitivity of the TCRE to two aspects of ocean ventilation: (i) the thickness of the ocean mixed layer setting the proportion of waters in direct contact with the atmosphere, and (ii) the ventilation timescale setting the rate of transfer of heat and carbon from the mixed layer to the ocean interior. Sensitivity experiments include varying the thickness of the mixed layer between a range of 50 to 300 m and the ventilation timescale between a range of 100 and 2000 years, and these changes occurring either separately or simultaneously (Table 1).

The box model with overturning is used to explore the climate response and the sensitivity of the TCRE to two further mechanisms that control the rate of ventilation of the ocean interior and extent of communication with the atmosphere: (i) the strength of the meridional overturning that sets the volume transport and transfer of heat and carbon into the deep ocean and (ii) the isolation fraction, δ, that controls the proportion of waters subducted in the Southern Ocean. Sensitivity experiments are conducted varying the Southern Ocean wind stress and the isolation fraction, and these changes are applied either separately or simultaneously (Table 1): the wind stress varies between 0.05 and 0.15 N m^{-2} corresponding to a variation of the pre-industrial overturning strength between 13 and 35 Sv, this range encapsulates the observed value of about 17 Sv for the Atlantic meridional overturning circulation (McCarthy et al. 2015); and the isolation fraction varies between 0.1 and 0.9, encapsulating a data-based estimate of δ of about 0.7 (Talley 1999) .

The 1D box model starts by design from a steady state since the model only solves for anomalies relative to its initial state. The box model with overturning is initialised with a prescribed atmospheric CO_2=280 ppm, temperature and dissolved inorganic carbon for the mixed layer in the low latitudes and the northern, the southern and deep ocean (Table 2), and a range of choices in the Southern Ocean wind stress that provides the Ekman upwelling in the Southern Ocean and the isolation fraction (Table 1). The model is integrated until the model transports, the thermocline thickness and its temperature and dissolved inorganic carbon all adjust to an equilibrium state (Appendix). The box model with overturning is simple enough to experience no significant model drift beyond a negligible truncation error and so the model reaches a real equilibrium state.

This pre-industrial equilibrium state differs for each ensemble (Table 2) and then forms the initial conditions for the model integrations with anthropogenic emissions.

Including anthropogenic emissions drives increasing radiative forcing and additional ocean heat supply, which in turn alters the volume of light water and the strength of the meridional overturning. The change in the meridional overturning, $\Delta q_{NA}(t)$, involving the volume transport from the upper ocean into the deep ocean in the high latitudes in the northern hemisphere, is related to the total ocean heat uptake averaged over the surface area of light water, $N(t)$ in W m^{-2}, by

$$\Delta q_{NA}(t) = \frac{N(t) A_{low}}{\rho_o C_{p,o} (T_{light}(t) - T_{deep}(t))}, \tag{3}$$

where this change in overturning equates to changes in the North Atlantic Deep Water formation; here A_{low} is the model area covered by the low latitudes, ρ_o is a referenced ocean density, $C_{p,o}$ is the specific heat capacity for the ocean, and T_{light} and T_{deep} are the temperatures of light waters in the low latitudes (mixed layer and thermocline) and of dense waters in the deep ocean respectively.

These changes in the strength of the meridional overturning, $q_{NA}(t)$ (Fig. 2a), drive subsequent changes in the Southern Ocean residual circulation involving a surface warming conversion into light waters in the southern high latitudes, $q_{so}(t)$ (Fig. 2b), and the diapycnal transfer in the low latitudes, $q_v(t)$ (Fig. 2c), which then collectively alter the thickness of the thermocline, $h_{therm}(t)$ (Fig. 2d). The meridional overturning weakens with the additional surface heating during emissions, but gradually recovers after emissions cease (Fig. 2). For simplicity, the climate feedback parameter is chosen to remain constant in our sensitivity experiments, and so does not alter with changes in the overturning, as instead explored by Winton et al. (2013) and Garuba et al. (2018).

3. Ocean mechanisms affecting the climate metric, the TCRE

The transient climate response to emissions, TCRE, defined by the ratio of the changes in global mean surface air temperature since the pre-industrial era, $\Delta T(t)$, to the cumulative carbon emissions, $I_{em}(t)$, may be interpreted as the product of a thermal contribution, $\Delta T(t)/R(t)$, and a carbon contribution, $R(t)/I_{em}(t)$ (Goodwin et al. 2015; Williams et al. 2016, 2017a; Katavouta et al. 2018):

$$\mathrm{TCRE} = \frac{\Delta T(t)}{I_{em}(t)} = \frac{\Delta T(t)}{R(t)} \frac{R(t)}{I_{em}(t)}, \tag{4}$$

where $R(t)$ is the radiative forcing.

The carbon contribution, $R(t)/I_{em}(t)$, is affected by the ocean carbon uptake as the radiative forcing, $R(t)$, is proportional to the logarithmic change in the atmospheric CO_2 relative to the pre-industrial, $R(t) = a\Delta \ln CO_2(t)$.

In both our models, during emissions (black solid lines in Fig.3a, c), there is an increase in both the atmosphere carbon inventory, ΔI_{atm}, (black dashed lines in Fig.3a, c) and the ocean carbon inventory, ΔI_{ocean}, (black dashed-dotted lines in Fig.3a, c), where Δ represents changes relative to the pre-industrial era. After emissions cease, the ocean carbon inventory increases at the expense of the atmospheric carbon inventory, as carbon is transferred into the ocean until a new global equilibrium is attained after typically 5000 years for a ventilation timescale of $\tau_{vent} = 1000$ y. This transfer of carbon from the atmosphere into the ocean corresponds to a general decrease in the carbon contribution, $R(t)/I_{em}(t)$, (red lines in Fig.3a, c) in time from the onset of emissions until a new equilibrium is reached.

The thermal contribution, $\Delta T(t)/R(t)$, may be understood in terms of the empirical global heat budget (2). The thermal contribution is controlled by the fraction of the radiative forcing, $R(t)$, directed towards surface warming and providing a radiative response, $\lambda \Delta T(t)$, rather than an increase in ocean heat content, $N(t)$.

In both our models, the radiative forcing increases during emissions and decreases after emissions cease (black solid lines in Fig.3b, d) following the changes in atmospheric CO_2. Initially most of the radiative forcing is directed towards warming the ocean and increasing ocean heat content, $N(t)$, (black dashed-dotted lines in Fig.3b, d). As the ocean interior warms, a larger fraction of the radiative forcing is instead directed towards surface warming (black dashed lines in Fig.3b, d). After emissions cease, ocean heat uptake gradually declines until the system reaches equilibrium when there is no further ocean heat uptake and all the radiative forcing is directed towards surface warming and providing a radiative response. This gradual decline in the fraction of the radiative forcing directed towards ocean heat uptake corresponds to a general increase in the thermal contribution, $\Delta T(t)/R(t)$ (red lines in Fig.3b, d), until a new equilibrium is attained.

For an atmosphere-ocean system at equilibrium, the climate response, $\Delta T(t_{eq})/I_{em}(t_{eq})$, is independent of the ocean ventilation and equal to $a/(\lambda I_B)$ (Williams et al. 2012), where I_B is the buffered atmosphere and ocean carbon inventory at the pre-industrial (Goodwin et al. 2007). However, during the transient period, the thermal and carbon contributions to the TCRE are controlled by how the ocean sequesters heat and carbon, and so the TCRE is a function of ocean ventilation. The effect of different ventilation processes altering the TCRE is investigated next.

a. Role of the thickness of the mixed layer

In our 1D box model, the mixed layer responds relatively rapidly to any forcing applied at the air-sea interface, compared with the response of the ocean interior. This fast response to emissions dominates the climate response during the beginning of the twentieth century (Held et al. 2010). A thick mixed layer leads to less atmospheric CO_2 and a smaller rise in surface air temperature, so that the TCRE and its carbon, $R(t)/I_{em}(t)$, and thermal, $\Delta T(t)/R(t)$, contributions are smaller (Fig. 4a, b and c).

The sensitivity of the TCRE (together with its thermal and carbon contributions) to the mixed-layer thickness is largest during the first decade after the start of emissions and then declines in time (Figs. 4a and 5a). After about a century, the TCRE dependence on the mixed-layer thickness is small and eventually, after 500 years, the TCRE becomes independent of the mixed-layer thickness (Fig. 5a middle and right panels).

The sensitivity of the thermal contribution for the TCRE to the mixed-layer thickness is generally larger than that of the carbon contribution (Figs. 4b,c, and 5b,c) as the ocean heat uptake is enhanced by its specific heat capacity, while the carbon uptake is inhibited by ocean buffering from carbonate chemistry.

b. Role of the ventilation timescale

In our 1D box model, the ventilation timescale controls the response of the ocean interior to atmospheric changes. A shorter ventilation timescale corresponds to a more rapid ventilation rate and an enhanced transfer of carbon and heat into the ocean interior. Hence, a shorter ventilation timescale leads to a smaller TCRE, and a smaller carbon, $R(t)/I_{em}(t)$, and thermal, $\Delta T(t)/R(t)$, contributions during the transient period before equilibrium (Fig. 4d, e and f).

The sensitivities of the carbon and thermal contributions to the ventilation rate operate on different timescales (Fig. 5b,c). On timescales of a decade to a century, the thermal contribution dominates the sensitivity of the TCRE, while on timescales of 500 years, the carbon contribution becomes more important. This difference in the sensitivities of the carbon and thermal contributions to the TCRE is due to the ocean heat and carbon uptake being controlled by different mechanisms operating on different timescales, such as involving the effects of heat storage and climate feedback versus carbon storage and ocean carbonate chemistry.

The TCRE sensitivity to the ventilation timescale is relatively small compared to the TCRE sensitivity to the thickness of the mixed layer during the first decade since the onset of emissions (Fig 5a left panel). After the first decade, the TCRE becomes more sensitive to the ventilation timescale and is further modified by the thickness of the mixed layer (Fig. 5a middle panel). On a timescale of 500 years, the TCRE only depends on the ventilation timescale (Fig. 5a right panel).

c. Role of the meridional overturning and isolation fraction

In the box model with overturning, the ventilation is affected by two mechanisms: the strength of overturning circulation and the extent of subduction in the Southern Ocean. The overturning circulation controls the exchange of water between the upper ocean and the deep ocean, and so alters the transfer of heat and carbon to the deep ocean. A stronger overturning is associated with an enhanced transfer of heat and carbon into the deep ocean, and so leads to a smaller TCRE and its carbon and thermal contributions (Fig. 6a, b and c), represented by $R(t)/I_{em}(t)$ and $\Delta T(t)/R(t)$, respectively.

The isolation fraction, δ, sets the proportion of waters subducted in the Southern Ocean relative to the total subduction rate. As δ increases, the proportion of waters subducted in the Southern Ocean increases, which reduces the communication with the atmosphere in the low latitudes and so reduces the uptake of heat and carbon there. In turn this reduced ocean heat and carbon uptake leads to a larger TCRE and carbon, $R(t)/I_{em}(t)$, and thermal, $\Delta T(t)/R(t)$, contributions (Fig. 6d, e and f). In addition, as δ increases, the thermocline waters become more isolated from the atmosphere and so the TCRE becomes less sensitive to the overturning strength (Fig. 7a).

The sensitivities of the carbon, $R(t)/I_{em}(t)$, and thermal, $\Delta T(t)/R(t)$, contributions to the strength of the overturning and the isolation fraction (Fig. 7b, c) operate in a similar manner to the sensitivities to the rate of ventilation in the 1D box model (Fig. 5b, c): the thermal contribution again dominates the sensitivity of the TCRE on timescales of decades to a century, while the carbon contribution becomes more important on timescales of 500 years.

4. Controls of the variability in the climate metric, the TCRE

The relative importance of the different ventilation mechanisms and emission scenarios in controlling the TCRE are now examined using ensemble experiments covering a wide parameter space (Table 1). The variability in the TCRE is quantified using the coefficient of variation, defined by the ratio of the standard deviation and mean for a given ensemble of model experiment with perturbed parameters at a particular time (Hawkins and Sutton 2009; Williams et al. 2017b).

A coefficient of variation is estimated for each of the four sets of ensembles with perturbation in either (i) the mixed-layer thickness, h_{ml}, (ii) the ventilation timescale, τ_{vent}, (iii) the strength of the overturning circulation altering with variations in the zonal wind stress in the Souther Ocean, τ_{wind}, or (iv) the proportion of water subducted in the Southern Ocean altering with the isolation fraction, δ (Table 1). This statistical measure is also evaluated for ensembles with several thousand members with combined perturbations in the input parameters for the 1D box model and the box model with overturning.

a. Effect of ocean ventilation on the TCRE variability

In the 1D box model, the variability of the TCRE due to the combined variability of the mixed-layer thickness and ventilation timescale is initially large, reduces over the next century, and subsequently increases over a couple of centuries before decreasing towards zero over several millennia (black line in Fig. 8a). On decadal timescales, the thickness of the mixed layer controls the variability of the TCRE, while on timescales of several decades to a century, there is a decreasing effect of mixed-layer thickness and an increasing importance of the ventilation timescale. Eventually after a couple of centuries, the ventilation timescale solely controls the variability of the TCRE (black lines in Fig. 8a, b and c).

The variability in the TCRE is dominated by the thermal contribution, $\Delta T(t)/R(t)$, on timescales from years to centuries, but is then dominated by the carbon contribution, $R(t)/I_{em}(t)$ (Fig. 8a,c). Over the first century, the variability in the thermal contribution generally decreases in time, while the variability in the carbon contribution slightly increases in time (red and blue lines in Fig. 8a). This trend in the variability of the TCRE and its thermal contribution is generally consistent with CMIP5 model diagnostics forced by a 1% increase in atmospheric CO_2 (Williams et al. 2017b). However, in the CMIP5 diagnostics, there is an initial large variability in the carbon contribution with a slight decreasing trend over the first 30 years since the pre-industrial, which is possibly due to effects of the terrestrial carbon uptake or from the pre-industrial conditions in CMIP5 models not being in equilibrium at the onset of emissions.

In the box model with overturning, the variability in the strength of the overturning and the isolation fraction contribute equally to the variability of the TCRE on timescales of some centuries (Fig. 8d, e, f), but the strength of overturning dominates on longer timescales. The thermal contribution again dominates the variability in the TCRE on timescales up to some centuries (red and blue lines in Fig.8d-f), but the carbon contribution becomes important on several centuries to millennia.

From this sensitivity analysis, the implications for understanding inter-model variability in the TCRE from Earth system models are that (i) on decadal timescales, inter-model differences in the thickness of the mixed layer are likely to be a major source of variability through their effect on ocean heat uptake, (ii) on timescales of decades to centuries, inter-model differences in the ventilation of heat are likely to be a major source of uncertainty from inter-model differences in the strength of overturning and mode water formation, and (iii) on centuries to millennia, inter-model differences in the carbon contribution become important due to differences in the overturning.

b. Effect of the carbon emissions on the TCRE variability

The sensitivity analysis is repeated for different rates and duration of carbon emissions to explore their interplay with the ventilated control of the TCRE (Fig. 9). The coefficient of variation for changes in the mixed-layer thickness is generally similar for these experiments with different carbon forcing (Fig. 9a).

The variability of the thermal contribution, $\Delta T(t)/R(t)$, due to changes in the ventilation timescale is effectively independent of the rate of carbon emissions and when emissions cease (red lines in Fig. 9b). However, the variability of the carbon contribution, $R(t)/I_{em}(t)$, due to changes in the ventilation timescale does alter with the rate of carbon emissions and the time when emissions cease. When there is more cumulative carbon emission, either from a larger emission rate or emissions ceasing later, the variability of the carbon contribution is smaller in the centuries after emissions ceasing (blue lines in Fig. 9b), which accordingly leads to the variability in the TCRE also being smaller (black lines in Fig. 9b).

This dependence of the variability in the carbon contribution to the rate and duration of carbon emissions is associated with the carbonate chemistry and changes in the buffering capacity of the ocean. A greater cumulative carbon emission from a larger emission rate or prolonged carbon emissions leads to a more acidic ocean surface during emissions, which alters the buffering capacity of the ocean. The ocean carbon uptake is then more controlled by these larger changes in buffering capacity, rather than by the variability from the physical changes in ventilation, such as from the ventilation timescale, the overturning strength and the isolation fraction (Fig. 9b, c and d).

The timescale of variability of different ocean ventilation processes for the TCRE and its thermal and carbon contribution are generally robust to changes in the strength of the emissions (Fig. 9), despite the strength of the carbon contribution varying with the cumulative carbon emission.

5. Discussion and summary

Sensitivity experiments are conducted using conceptual atmosphere-ocean models to understand how different aspects of ocean ventilation influence the climate metric, the Transient Climate Response to cumulative carbon emissions (TCRE), and its thermal and carbon contributions. In our experiments, the variability in the TCRE from ocean ventilation is dominated on timescales of years to centuries by the thermal response and on timescales of centuries to millennia by the carbon response. The effect of the ventilation is primarily controlled by the thickness of the mixed layer on timescales of years to decades and then gradually switches to being controlled by the rate of ventilation of the ocean thermocline and deep ocean on timescales of several decades and longer. This rate of ventilation of the ocean interior is itself affected by both the variability in the Atlantic meridional overturning circulation and the extent of subduction in the Southern Ocean, with the variability in the meridional overturning circulation dominating on timescales of several centuries and longer.

Idealised one-dimensional box models have been extensively used to understand the thermal contribution of the ocean to the climate response to carbon emissions (Wigley and Schlesinger 1985; Gregory 2000; Held et al. 2010; Geoffroy et al. 2012; Kostov et al. 2014), together with a more limited use of conceptual models including a physical representation of overturning (Marshall and Zanna 2014). However, unlike previous studies, our models solve for changes in the ocean heat and carbon budgets due to carbon emissions and hence allow the sensitivity of the climate metric, the TCRE, to be assessed. Similarly to previous studies, the thermal response to changes in radiative forcing undertakes a fast adjustment associated with the ocean mixed layer on timescales of years to decades and a slow adjustment associated with the ventilation of the ocean interior on timescales of decades to many centuries (Gregory 2000; Held et al. 2010). However, unlike previous studies, we demonstrate that the carbon response to carbon emissions also undertakes a fast adjustment associated with the response of the ocean mixed layer and a slow adjustment associated with the ventilation of the ocean interior. This slow adjustment of the carbon response becomes important in controlling variability in the TCRE on timescales of several centuries to millennia. For the slow and fast responses, the timescales for the thermal and carbon adjustment are not the same as they involve different effects for the thermal response from ocean heat uptake and climate feedback and for the carbon response from ocean carbon uptake and ocean carbonate chemistry.

Our sensitivity experiments suggest that the inter-model variability in the TCRE for Earth system models is partly controlled by differences in ocean ventilation, associated with the thickness of the mixed layer and the rate of ventilation of the ocean interior. Changes in the ocean circulation redistribute the heat in the ocean and modify the pattern of sea surface warming (Banks and Gregory 2006; Xie and Vallis 2012; Garuba and Klinger 2016). This dynamic effect from the evolution of the overturning circulation with warming is captured in our box model with overturning and so our experiments include this effect on the TCRE. However, our model omits any connection between the pattern of sea surface warming and the cloud cover and climate feedbacks (Rose et al. 2014; Rugenstein et al. 2016; Trossman et al. 2016; Ceppi and Gregory 2017; Andrews and Webb 2018). Our model also ignores the time evolution of the climate feedbacks (Andrews et al. 2012) associated with the changes in the pattern of surface warming (Armour et al. 2013; Andrews et al.

2015). These changes in the climate feedbacks with the evolving pattern of sea surface warming contribute further to inter-model variability in Earth system models.

Our box model with overturning only provides a crude representation of the Southern Ocean, a region of enhanced anthropogenic ocean heat and carbon uptake that is highly variable amongst the Earth system models (Frölicher et al. 2015). The fraction of isolation in our conceptual model is meant to represent the variability in intermediate and sub-Antarctic mode water formation, but omits changes in Antarctic bottom water formation. Our conceptual models only include the atmosphere and ocean, so omit the effect of the terrestrial system, which strongly varies within Earth system models (Arora et al. 2013; Friedlingstein et al. 2014) and drives much of the variability in the carbon contribution to the TCRE (Williams et al. 2017b). However, after emissions cease, the terrestrial uptake of carbon will decline (e.g. Williams et al. 2017a) and the variability in the ocean carbon uptake is expected instead to dominate on timescales of many centuries and longer. Our conceptual models also omit ocean biology and calcium carbonate cycling. While inter-model differences in the representation of ocean biology affect the regional ocean carbon response, their global contribution turns out to be minor on centennial timescales. Likewise inter-model variability in calcium carbonate cycling and sediment changes only becomes important in affecting the amount of atmospheric CO_2 and modifying the climate response on timescales of several millennia (Archer 2005; Goodwin et al. 2009).

While our conceptual study makes simplifying assumptions, our aim is to reveal the importance of the separate physical processes contributing to ocean ventilation and their effect on the climate response to carbon emissions on timescales of years to many centuries. In a realistic Earth system model, the different contributions to ocean ventilation from mixed-layer thickness and circulation changes all occur in an inter-connected manner. However, in our conceptual model, the different ventilation contributions are imposed in a separate manner to reveal the relative importance of changes in mixed-layer thickness and ventilation rate of the ocean interior including the effects of the strength of the meridional overturning and the extent of Southern Ocean mode water formation. By adopting a conceptual model, our ventilation study is also able to span a wide parameter space using a large number of ensembles. Our ensemble analysis suggests that inter-model differences in the TCRE from ocean ventilation are dominated by thermal processes on timescales of years to several centuries and by differences in ocean carbon uptake on timescales of several centuries and longer. Hence, the study provides mechanistic insight into how ocean ventilation affects the climate response during emissions and after emissions cease, as well as providing a well-posed reference point to interpret inter-model variability in the response of complex Earth systems to climate forcing.

Acknowledgments. This work was supported by a UK Natural Environmental Research Council grant NE/N009789/1. This manuscript benefited from constructive comments from three referees.

APPENDIX

Appendix: Box model with overturning

Volume budget

The dynamics of the box model with overturning is based on the model by Gnanadesikan (1999) (black solid lines and black arrows in Fig. 1b). The thickness of the light water, $h(t)$, is set by the volume balance between the volume transports associated with sinking in the northern high latitudes, $q_{NA}(t)$, diapycnal upwelling in the low latitudes, $q_v(t)$, and the residual circulation involving the Ekman upwelling in the southern high latitudes driven by winds and the return flow due to baroclinic eddies, $q_{so}(t) = q_{Ekman} + q_{eddy}(t)$, such that

$$A_{low}\frac{dh(t)}{dt} = q_{NA}(t) + q_v(t) + q_{so}(t), \tag{A1}$$

where $A_{low} = 2 \times 10^{14}$ m^2 is the area covered by the low latitudes.

The volume transport associated with the Ekman upwelling, q_{Ekman}, is specified as

$$q_{Ekman} = \frac{\tau_{wind} L_x}{\rho_o f}, \tag{A2}$$

where $L_x = 30000$ km is the zonal extent of Southern Ocean, $\rho_o = 1025$ kg m^{-3} is a referenced ocean density, f is the Coriolis parameter and τ_{wind} is the zonal wind stress varying in the sensitivity experiments from 0.05 to 0.15 N m^{-2} encapsulating the typical value of 0.1 N m^{-2} for the wind stress; this typical value of the wind stress is expected to be somewhat larger in the Southern Ocean.

The volume transport associated with the baroclinic eddies in the Southern Ocean, $q_{eddy}(t)$, is parametrised as

$$q_{eddy}(t) = -\frac{k_{eddy} L_x h(t)}{L_y}, \tag{A3}$$

where $k_{eddy} = 10^3$ m^2 s^{-1} is the eddy diffusion coefficient, and $L_y = 1500$ km is the meridional extent of the Southern Ocean.

The volume transport associated with the diapycnal upwelling, $q_v(t)$, is parametrised as

$$q_v(t) = \frac{A_{low} k_v}{h(t)}, \tag{A4}$$

where $k_v = 10^{-5}$ m^2 s^{-1} is the diapycnal mixing coefficient.

The volume transport associated with the sinking in the northern high latitudes, $q_{NA}(t)$ is parametrised as

$$q_{NA}(t) = -\frac{g'}{2f} h(t_o)^2 + \Delta q_{NA}(t), \tag{A5}$$

where $g' = 0.02$ m s^{-2} is the reduced gravity, t_o is the pre-industrial era and Δ is the change relative to the pre-industrial. The changes in the volume transport associated with the sinking in the northern latitudes, $\Delta q_{NA}(t)$, are controlled by the ocean heat uptake due to anthropogenic emissions, $N(t)$, and the temperature contrast between the light and dense waters in the low latitudes, $T_{light}(t) - T_{deep}(t)$, as described by (3) and so (A5) becomes

$$q_{NA}(t) = -\frac{g'}{2f}h(t_o)^2 + \frac{N(t)A_{low}}{\rho_o C_{p,o}(T_{light}(t) - T_{deep}(t))}. \tag{A6}$$

The model is initialised with a random thickness of light waters, h, and integrated to a steady state, which provides the volume transports and the thickness of the thermocline in low latitudes in the pre-industrial era, $h(t_o)$ (Table 2). The volume transports and the upper ocean thickness, $h(t)$, evolve with warming due to emissions according to (A1) to (A6) (Fig. 2). The total ocean depth is assumed constant and equal to 4000 m. The deep ocean thickness in the low latitudes evolves following the changes in the upper ocean thickness.

Thermal and carbon budgets

There is air-sea exchange of heat and carbon between the slab atmosphere and the upper ocean. In the low latitudes, the upper ocean consists of a layer of light water separated into two layers (Fig.1b): a mixed layer with fixed thickness, $h_{ml} = 100$ m, and a thermocline layer with varying thickness set by the volume transports, $h_{therm}(t) = h(t) - h_{ml}$. In the high latitudes, the upper ocean is represented by boxes for the Southern Ocean and the northern high latitudes, both with fixed thicknesses of $h_{high} = 1000$ m.

The model is initialised and run to thermal and carbon equilibrium where there is no net ocean heat and carbon uptake and the heat and carbon divergence at each of the ocean boxes in contact with the atmosphere are balanced by heat and carbon fluxes from the atmosphere. This pre-industrial state has (i) higher dissolved inorganic carbon in the high latitudes and the deep ocean, and ocean carbon uptake in the northern high latitudes and ocean carbon release in the low latitudes, and (ii) higher temperature in the upper ocean in the low latitudes, and ocean heat uptake at the low latitudes and ocean heat release at the northern high latitudes. An example of the model pre-industrial ocean heat and carbon distribution is shown in Table 2.

The discrete form of the divergence theorem is used to express the heat and carbon budgets. The budget for a scalar C such as temperature or dissolved inorganic carbon of a box/layer is expressed as

$$\frac{d}{dt}\left(C_{box}(t)V_{box}(t)\right) = -\int_{box} \nabla\cdot\left(C(t)\vec{v}(t)\right)dV + \mathrm{S}_C(t), \tag{A7}$$

where $\vec{v}(t)$ is the velocity of the flow into the box, V is the volume and S_C is a source/sink of C, for example representing the supply of C from the atmosphere into the ocean. The discrete form of the divergence theorem for this box is expressed as

$$\int_{box} \nabla\cdot(C\vec{v})\,dV = \oint_{box} C\vec{v}\cdot d\vec{S} = -\underset{box}{\Delta}(Cq), \tag{A8}$$

where S is the boundary surface of the volume V with $d\vec{S}$ being outward pointing, q is a volume transport through the boundary surface of the box and is positive into the box, and $\underset{box}{\Delta}$ notes the transports of C into the box minus the transports of C out of the box. The change in the sign when using $\underset{box}{\Delta}$ is due to the transport being defined positive into the box. As an example for the deep ocean, $\underset{deep}{\Delta}(C(t)q(t)) = -(q_{NA}(t)C_N(t) + q_{SO}(t)C_{deep}(t) + q_v(t)C_{deep}(t))$, which represents that the total convergence of C in the deep ocean box is equal to the amount of the scalar C sinking in the northern high latitudes into the deeper ocean (with q_{NA} being negative) minus the amount of the tracer C returning from the deep ocean into the upper ocean either in the Southern Ocean or in the low latitudes by diapycnal transfer.

Using (A7) and (A8), the budget for a scalar C becomes

$$\frac{d}{dt}\left(C_{box}(t)V_{box}(t)\right) = \underset{box}{\Delta}\left(C(t)q(t)\right) + \mathrm{S}_C(t). \tag{A9}$$

This discrete form of the budget given by (A9) is used to express the heat and carbon budgets in the model.

The changes in the heat budget for the global model driven by the radiative forcing, R, are described by

$$\rho_a C_{p,a} A h_{atm} \frac{d}{dt}\left(T_{atm}(t)\right) + \rho_o C_{p,o} \sum_{box}^{ocean} \frac{d}{dt}\left(T_{box}(t)V_{box}(t)\right) = AN_{TOA}(t), \tag{A10a}$$

$$\rho_a C_{p,a} A h_{atm} \frac{d}{dt}\left(T_{atm}(t)\right) = A\left(N_{TOA}(t) - N(t)\right), \tag{A10b}$$

$$\rho_o C_{p,o} \sum_{box}^{ocean} \frac{d}{dt}\left(T_{box}(t)V_{box}(t)\right) = AN(t), \tag{A10c}$$

$$N(t) = \frac{1}{A}\sum_{box}^{ocean}\left(A_{box}N_{box}(t)\right), \tag{A10d}$$

with the changes in the heat budget of each individual box being described by

$$\rho_o C_{p,o} \frac{d}{dt}\left(T_{box}(t)V_{box}(t)\right) = \rho_o C_{p,o} \underset{box}{\Delta}\left(q(t)T(t)\right) + A_{box}N_{box}(t), \tag{A11}$$

where subscript *box* indicates the different ocean boxes/layers in the model, $A = \sum_{box}^{ocean} A_{box}$ is the area of the ocean, equal to the area of the atmosphere, h_{atm} is the thickness of the slab atmosphere, $T_{atm}(t)$ in K is the temperature of the slab atmosphere, $q(t)$ is the volume transport in Sv, $T_{box}(t)$ in K is the ocean temperature for each ocean box, $N_{box}(t)$ and $N(t)$ in Wm^{-2} are the heat flux from the atmosphere into each ocean box and into the entire ocean, respectively, with N_{therm} and N_{deep} being zero as the thermocline and the deep ocean are not in direct contact with the atmosphere, $N_{TOA}(t)$ in Wm^{-2} is the net downward heat flux entering the system at the top of the atmosphere in response to the carbon emissions, $\rho_a = 1$ kg m^{-3} and $\rho_o = 1025$ kg m^{-3} are a referenced atmosphere and ocean density, respectively, and $C_{p,a} = 1000$ J kg^{-1} K^{-1} and $C_{p,o} = 4000$ J kg^{-1} K^{-1} are the specific heat capacities for the atmosphere and ocean, respectively. There is no net ocean heat uptake in the pre-industrial, $N(t_o) = 0$, and the ocean heat uptake due to the increase in radiative forcing, $N(t) - N(t_o) = N(t)$, is distributed equally over the ocean surface area. The net downward heat flux, $N_{TOA}(t)$, and the instantaneous flux of heat from the ocean into the atmosphere (defined as positive upwards), $N_{TOA}(t) - N(t)$, in response to the carbon emissions, are expressed as

$$N_{TOA}(t) = R(t) - \lambda \Delta T_{atm}(t), \tag{A12a}$$

$$N_{TOA}(t) - N(t) = c(\Delta T_{surf}(t) - \Delta T_{atm}(t)), \tag{A12b}$$

where λ in W m^{-2} K^{-1} is the climate feedback parameter, c in W m^{-2} K^{-1} is an air-sea heat transfer parameter, Δ is the change relative to the pre-industrial, and $T_{surf}(t)$ in K is the temperature of the ocean surface, which is defined by an area-weighted average of the temperature for the boxes in contact with the atmosphere. In the main text, T_{atm} is referred to as T for simplicity.

The changes in the carbon budget of the global model driven by the imposed carbon emissions, $F_{em}(t)$ in mol C m^{-2}s^{-1} are described by

$$M_a \frac{d}{dt}\left(CO_2(t)\right) + \rho_o \sum_{box}^{ocean} \frac{d}{dt}\left(DIC_{box}(t) V_{box}(t)\right) = AF_{em}(t), \tag{A13a}$$

$$M_a \frac{d}{dt}\left(CO_2(t)\right) = A(F_{em}(t) - F(t)), \tag{A13b}$$

$$\rho_o \sum_{box}^{ocean} \frac{d}{dt}\left(DIC_{box}(t) V_{box}(t)\right) = AF(t), \tag{A13c}$$

$$F(t) = \frac{1}{A} \sum_{box}^{ocean} \left(A_{box} F_{box}(t)\right), \tag{A13d}$$

with the changes in the carbon budget of each individual box being described by

$$\rho_o \frac{d}{dt}\left(DIC_{box}(t) V_{box}(t)\right) = \rho_o \underset{box}{\Delta}\left(q(t) DIC(t)\right) + A_{box} F_{box}(t), \tag{A14}$$

where $CO_2(t)$ is the atmospheric CO_2, M_a is the number of moles of gas in the atmosphere, $DIC_{box}(t)$ in mol C kg^{-1} is the dissolved inorganic carbon for each ocean box, $F_{box}(t)$ and $F(t)$

in mol C $m^{-2}s^{-1}$ are the carbon flux from the atmosphere into each ocean box and into the entire ocean, respectively, with F_{therm} and F_{deep} being zero as the thermocline and the deep ocean are not in direct contact with the atmosphere. There is no net ocean carbon uptake in the pre-industrial, $F(t_o) = 0$, and the ocean carbon uptake due to the carbon emissions, $F(t) - F(t_o) = F(t)$, is distributed equally over the ocean surface area, and is expressed as

$$F(t) = \rho_o K_g \left(K_o(t) CO_2(t) - [CO_2(t)]_{surf} \right), \tag{A15}$$

where K_g in m s^{-1} is the air-sea gas transfer coefficient, $K_o(t)$ in mol C kg^{-1} is the solubility of carbon in the ocean water and $[CO_2(t)]_{surf}$ in mol C kg^{-1} is the dissolved CO_2 at the ocean surface. The dissolved CO_2 at the ocean surface is estimated based on the partitioning of the dissolved inorganic carbon at the surface using the iterative algorithm of Follows et al. (2006) by ignoring changes in biology or weathering, and by assuming the total alkalinity remains constant. This partitioning method accounts for the evolution of the ocean carbon equilibrium coefficients with changes in temperature and solves for the changes in the ocean *pH* with changes in the dissolved CO_2. The surface *DIC* of the ocean is defined from a volume weighting of the *DIC* in the boxes in contact with the atmosphere.

A summary for the values of parameters in the box model with overturning that are kept constant in the sensitivity experiment is provided in the supplementary information.

References

Allen, M. R., D. J. Frame, C. Huntingford, C. D. Jones, J. A. Lowe, M. Meinshausen, and N. Meinshausen, 2009: Warming caused by cumulative carbon emissions towards the trillionth tonne. *Nature*, **458**, 1163–1166, doi:10.1038/nature08019.

Andrews, T., J. M. Gregory, and M. J. Webb, 2015: The dependence of radiative forcing and feedback on evolving patterns of surface temperature change in climate models. *Journal of Climate*, **28 (4)**, 1630–1648, doi:10.1175/JCLI-D-14-00545.1.

Andrews, T., J. M. Gregory, M. J. Webb, and K. E. Taylor, 2012: Forcing, feedbacks and climate sensitivity in CMIP5 coupled atmosphere-ocean climate models. *Geophysical Research Letters*, **39 (9)**, doi:10.1029/2012GL051607.

Andrews, T., and M. J. Webb, 2018: The dependence of global cloud and lapse rate feedbacks on the spatial structure of tropical Pacific warming. *Journal of Climate*, **31 (2)**, 641–654, doi:10.1175/JCLI-D-17-0087.1.

Archer, D., 2005: Fate of fossil fuel CO_2 in geologic time. *Journal of Geophysical Research: Oceans*, **110 (C9)**, doi:10.1029/2004JC002625.

Armour, K. C., C. M. Bitz, and G. H. Roe, 2013: Time-varying climate sensitivity from regional feedbacks. *Journal of Climate*, **26 (13)**, 4518–4534, doi:10.1175/JCLI-D-12-00544.1.

Arora, V. K., and Coauthors, 2013: Carbon-concentration and carbon-climate feedbacks in CMIP5 Earth system models. *Journal of Climate*, **26 (15)**, 5289–5314, doi:10.1175/JCLI-D-12-00494.1.

Banks, H. T., and J. M. Gregory, 2006: Mechanisms of ocean heat uptake in a coupled climate model and the implications for tracer based predictions of ocean heat uptake. *Geophysical Research Letters*, **33 (7)**, doi:10.1029/2005GL025352.

Ceppi, P., and J. M. Gregory, 2017: Relationship of tropospheric stability to climate sensitivity and Earth's observed radiation budget. *Proceedings of the National Academy of Sciences*, **114 (50)**, 13 126–13 131, doi:10.1073/pnas.1714308114.

Cheng, W., J. C. H. Chiang, and D. Zhang, 2013: Atlantic meridional overturning circulation (AMOC) in CMIP5 models: RCP and historical simulations. *Journal of Climate*, **26 (18)**, 7187–7197, doi:10.1175/JCLI-D-12-00496.1.

Church, J. A., and Coauthors, 2011: Revisiting the Earth's sea-level and energy budgets from 1961 to 2008. *Geophysical Research Letters*, **38 (18)**, L18 601, doi:10.1029/2011GL048794.

Follows, M. J., T. Ito, and S. Dutkiewicz, 2006: On the solution of the carbonate chemistry system in ocean biogeochemistry models. *Ocean Modelling*, **12**, 290–301, doi:https://doi.org/10.1016/j.ocemod.2005.05.004.

Forster, P. M., T. Andrews, P. Good, J. M. Gregory, L. S. Jackson, and M. Zelinka, 2013: Evaluating adjusted forcing and model spread for historical and future scenarios in the CMIP5 generation of climate models. *Journal of Geophysical Research: Atmospheres*, **118 (3)**, 1139–1150, doi:10.1002/jgrd.50174.

Friedlingstein, P., M. Meinshausen, V. K. Arora, C. D. Jones, A. Anav, S. K. Liddicoat, and R. Knutti, 2014: Uncertainties in CMIP5 climate projections due to carbon cycle feedbacks. *Journal of Climate*, **27 (2)**, 511–526, doi:10.1175/JCLI-D-12-00579.1.

Frölicher, T. L., J. L. Sarmiento, D. J. Paynter, J. P. Dunne, J. P. Krasting, and M. Winton, 2015: Dominance of the Southern Ocean in anthropogenic carbon and heat uptake in CMIP5 models. *Journal of Climate*, **28 (2)**, 862–886, doi:10.1175/JCLI-D-14-00117.1.

Garuba, O. A., and B. A. Klinger, 2016: Ocean heat uptake and interbasin transport of the passive and redistributive components of surface heating. *Journal of Climate*, **29 (20)**, 7507–7527, doi:10.1175/JCLI-D-16-0138.1.

Garuba, O. A., J. Lu, F. Liu, and H. A. Singh, 2018: The active role of the ocean in the temporal evolution of climate sensitivity. *Geophysical Research Letters*, **45 (1)**, 306–315, doi:10.1002/2017GL075633.

Geoffroy, O., D. Saint-Martin, and A. Ribes, 2012: Quantifying the sources of spread in climate change experiments. *Geophysical Research Letters*, **39 (24)**, doi:10.1029/2012GL054172.

Gillet, N. P., V. K. Arora, D. Matthews, and M. R. Allen, 2013: Constraining the ratio of global warming to cumulative CO_2 emissions using CMIP5 simulations. *Journal of Climate*, **26**, 6844–6858, doi:10.1175/JCLI-D-12-00476.1.

Gnanadesikan, A., 1999: A simple predictive model of the structure of the oceanic pycnocline. *Science*, **283**, 2077–2081, doi:10.1126/science.283.5410.2077.

Goodwin, P., R. G. Williams, M. J. Follows, and S. Dutkiewicz, 2007: Ocean-atmosphere partitioning of anthropogenic carbon dioxide on centennial timescales. *Global Biogeochemical Cycles*, **21 (1)**, GB1014, doi:10.1029/2006GB002810.

Goodwin, P., R. G. Williams, and A. Ridgwell, 2015: Sensitivity of climate to cumulative carbon emissions due to compensation of ocean heat and carbon uptake. *Nature Geoscience*, **8**, 29–34, doi:10.1038/ngeo2304.

Goodwin, P., R. G. Williams, R. G. Ridgwell, and M. J. Follows, 2009: Climate sensitivity to the carbon cycle modulated by past and future changes to ocean chemistry. *Nature Geoscience*, **2**, 145–150, doi:10.1038/ngeo416.

Gregory, J. M., 2000: Vertical heat transports in the ocean and their effect on time-dependent climate change. *Climate Dynamics*, **16**, 501–515, doi:10.1007/s003820000059.

Gregory, J. M., and P. M. Forster, 2008: Transient climate response estimated from radiative forcing and observed temperature change. *Journal of Geophysical Research: Atmospheres*, **113**, D23 105, doi:10.1029/2008JD010405.

Gregory, J. M., and Coauthors, 2004: A new method for diagnosing radiative forcing and climate sensitivity. *Geophysical Research Letters*, **31 (3)**, L03 205, doi:10.1029/2003GL018747.

Gregory, J. M., and Coauthors, 2005: A model intercomparison of changes in the Atlantic thermohaline circulation in response to increasing atmospheric CO_2 concentration. *Geophysical Research Letters*, **32 (12)**, doi:10.1029/2005GL023209.

Hawkins, E., and R. Sutton, 2009: The potential to narrow uncertainty in regional climate predictions. *Bulletin of the American Meteorological Society*, **90 (8)**, 1095–1108, doi:10.1175/2009BAMS2607.1.

Held, I. M., M. Winton, K. Takahashi, T. Delworth, F. Zeng, and G. K. Vallis, 2010: Probing the fast and slow components of global warming by returning abruptly to preindustrial forcing. *Journal of Climate*, **23 (9)**, 2418–2427, doi:10.1175/2009JCLI3466.1.

Johnson, H. L., D. P. Marshall, and D. A. J. Sproson, 2007: Reconciling theories of a mechanically driven meridional overturning circulation with thermohaline forcing and multiple equilibria. *Climate Dynamics*, **29 (7)**, 821–836, doi:10.1007/s00382-007-0262-9.

Katavouta, A., R. G. Williams, P. Goodwin, and V. Roussenov, 2018: Reconciling atmospheric and oceanic views of the Transient Climate Response to Emissions. *Geophysical Research Letters*, **45 (12)**, 6205–6214, doi:10.1029/2018GL077849.

Kostov, Y., K. C. Armour, and J. Marshall, 2014: Impact of the Atlantic meridional overturning circulation on ocean heat storage and transient climate change. *Geophysical Research Letters*, **41 (6)**, 2108–2116, doi:10.1002/2013GL058998.

MacDougall, A. H., N. C. Swart, and R. Knutti, 2017: The uncertainty in the transient climate response to cumulative CO_2 emissions arising from the uncertainty in physical climate parameters. *Journal of Climate*, **30 (2)**, 813–827, doi:10.1175/JCLI-D-16-0205.1.

Marshall, D. P., and L. Zanna, 2014: A conceptual model of ocean heat uptake under climate change. *Journal of Climate*, **27 (22)**, 8444–8465, doi:10.1175/JCLI-D-13-00344.1.

Matthews, H. D., N. P. Gillett, P. A. Stott, and K. Zickfeld, 2009: The proportionality of global warming to cumulative carbon emissions. *Nature*, **459**, 829–833, doi:10.1038/nature08047.

McCarthy, G., and Coauthors, 2015: Measuring the Atlantic Meridional Overturning Circulation at 26^{o}N. *Progress in Oceanography*, **130**, 91 – 111, doi:https://doi.org/10.1016/j.pocean.2014.10.006.

Myhre, G., E. J. Highwood, K. P. Shine, and F. Stordal, 1998: New estimates of radiative forcing due to well mixed greenhouse gases. *Geophysical Research Letters*, **25**, 2715–2718, doi:10.1029/98GL01908.

Raper, S. C. B., J. M. Gregory, and R. J. Stouffer, 2002: The role of climate sensitivity and ocean heat uptake on AOGCM transient temperature response. *Journal of Climate*, **15 (1)**, 124–130, doi:10.1175/1520-0442(2002)015⟨0124:TROCSA⟩2.0.CO;2.

Roemmich, D., J. Church, J. Gilson, D. Monselesan, P. Sutton, and S. Wijffels, 2015: Unabated planetary warming and its ocean structure since 2006. *Nature Climate Change*, **5 (3)**, 240, doi:https://doi.org/10.1038/nclimate2513.

Rose, B. E. J., K. C. Armour, D. S. Battisti, N. Feldl, and D. D. B. Koll, 2014: The dependence of transient climate sensitivity and radiative feedbacks on the spatial pattern of ocean heat uptake. *Geophysical Research Letters*, **41 (3)**, 1071–1078, doi:10.1002/2013GL058955.

Rugenstein, M. A., K. Caldeira, and R. Knutti, 2016: Dependence of global radiative feedbacks on evolving patterns of surface heat fluxes. *Geophysical Research Letters*, **43 (18)**, 9877–9885, doi:10.1002/2016GL070907.

Rugenstein, M. A. A., M. Winton, R. J. Stouffer, S. M. Griffies, and R. Hallberg, 2013: Northern high-latitude heat budget decomposition and transient warming. *Journal of Climate*, **26 (2)**, 609–621, doi:10.1175/JCLI-D-11-00695.1.

Sabine, C. L., and Coauthors, 2004: The oceanic sink for anthropogenic CO_2. *Science*, **305 (5682)**, 367–371, doi:10.1126/science.1097403.

Solomon, S., G.-K. Plattner, R. Knutti, and P. Friedlingstein, 2009: Irreversible climate change due to carbon dioxide emissions. *Proc. Natl. Acad. Sci. USA*, **106**, 1704–1709, doi:10.1073/pnas.0812721106.

Talley, L. D., 1999: Some aspects of ocean heat transport by the shallow, intermediate and deep overturning circulations. *Mechanisms of Global Climate Change at Millennial Time Scales*, P. U. Clark and R. S. Webb and L. D. Keigwin, 1–22, doi:10.1029/GM112p0001.

Trossman, D. S., J. B. Palter, T. M. Merlis, Y. Huang, and Y. Xia, 2016: Large-scale ocean circulation-cloud interactions reduce the pace of transient climate change. *Geophysical Research Letters*, **43 (8)**, 3935–3943, doi:10.1002/2016GL067931.

Wigley, T. M. L., and M. E. Schlesinger, 1985: Analytical solution for the effect of increasing CO_2 on global mean temperature. *Nature*, **315**, 649–652, doi:10.1038/315649a0.

Williams, R. G., P. Goodwin, A. Ridgwell, and P. L. Woodworth, 2012: How warming and steric sea level rise relate to cumulative carbon emissions. *Geophysical Research Letters*, **39**, L19 715, doi:10.1029/2012GL052771.

Williams, R. G., P. Goodwin, V. M. Roussenov, and L. Bopp, 2016: A framework to understand the Transient Climate Response to Emissions. *Environmental Research Letters*, **11**, doi:10.1088/1748-9326/11/1/015003.

Williams, R. G., V. Roussenov, T. L. Frölicher, and P. Goodwin, 2017a: Drivers of continued surface warming after the cessation of carbon emissions. *Geophysical Research Letters*, **44**, 10,633–10,642, doi:10.1002/2017GL075080.

Williams, R. G., V. Roussenov, P. Goodwin, L. Resplandy, and L. Bopp, 2017b: Sensitivity of global warming to carbon emissions: Effects of heat and carbon uptake in a suite of Earth system models. *Journal of Climate*, **30 (23)**, 9343–9363, doi:10.1175/JCLI-D-16-0468.1.

Winton, M., S. M. Griffies, B. L. Samuels, J. L. Sarmiento, and T. L. Frölicher, 2013: Connecting changing ocean circulation with changing climate. *Journal of Climate*, **26 (7)**, 2268–2278, doi:10.1175/JCLI-D-12-00296.1.

Xie, P., and G. K. Vallis, 2012: The passive and active nature of ocean heat uptake in idealized climate change experiments. *Climate Dynamics*, **38 (3)**, 667–684, doi:10.1007/s00382-011-1063-8.

Zickfeld, K., M. Eby, H. D. Matthews, and A. J. Weaver, 2009: Setting cumulative emissions targets to reduce the risk of dangerous climate change. *Proc. Natl. Acad. Sci. USA*, **106**, 16 129–16 134, doi:10.1073/pnas.0805800106.

LIST OF TABLES

Table 1. Sensitivity experiments: parameter space of the model ensembles. The ventilation timescale sets the rate of ventilation of the ocean interior in the 1D box model. The Southern Ocean wind stress sets the strength of the overturning circulation. The isolation fraction sets the proportion of water that is subducted in the Southern Ocean. Note that the experiment with variations in both the mixed layer and the ventilation timescale consists of 4896 ensembles (51×96 ensembles) and the experiment with variations in both Southern Ocean wind stress and isolation fraction consists of 8181 ensembles (101×81 ensembles). . . . 36

Table 2. Pre-industrial state in the box model with overturning for different choices of Southern Ocean wind stress, τ_{wind}, and isolation fraction, δ. The pre-industrial atmospheric $CO_2 = 280$ ppm is prescribed in all the ensembles. The pre-industrial distribution of heat and carbon, and the volume transports vary in the sensitivity experiments, so as an example values from three ensembles are presented. Subscripts N, S, $deep$, ml and $therm$ note the southern high latitude, the northern high latitude, the deep ocean, the mixed layer and the thermocline, respectively. Here the flux of heat and carbon into the ocean is shown in W and mol s^{-1} to highlight the thermal and carbon equilibrium state in the pre-industrial. 37

TABLE 1. Sensitivity experiments: parameter space of the model ensembles. The ventilation timescale sets the rate of ventilation of the ocean interior in the 1D box model. The Southern Ocean wind stress sets the strength of the overturning circulation. The isolation fraction sets the proportion of water that is subducted in the Southern Ocean. Note that the experiment with variations in both the mixed layer and the ventilation timescale consists of 4896 ensembles (51×96 ensembles) and the experiment with variations in both Southern Ocean wind stress and isolation fraction consists of 8181 ensembles (101×81 ensembles).

variable	lower limit	upper limit	interval of variation	number of ensembles
		1D box model		
mixed-layer thickness (h_{ml})	50 m	300 m	5 m	51
ventilation timescale (τ_{vent})	100 y	2000 y	20 y	96
		box model with overturning		
Southern Ocean wind stress (τ_{wind})	0.05 N m^{-2}	0.15 N m^{-2}	0.001 N m^{-2}	101
isolation fraction (δ)	10%	90%	1%	81

TABLE 2. Pre-industrial state in the box model with overturning for different choices of Southern Ocean wind stress, τ_{wind}, and isolation fraction, δ. The pre-industrial atmospheric $CO_2 = 280$ ppm is prescribed in all the ensembles. The pre-industrial distribution of heat and carbon, and the volume transports vary in the sensitivity experiments, so as an example values from three ensembles are presented. Subscripts N, S, $deep$, ml and $therm$ note the southern high latitude, the northern high latitude, the deep ocean, the mixed layer and the thermocline, respectively. Here the flux of heat and carbon into the ocean is shown in W and mol s^{-1} to highlight the thermal and carbon equilibrium state in the pre-industrial.

variable	τ_{wind}=0.05 N m^{-2}, δ=50%	τ_{wind}=0.1 N m^{-2}, δ=50%	τ_{wind}=0.1 N m^{-2}, δ=90%
northern sinking, $q_{NA}(t_o)$	13 Sv	23.7 Sv	23.7 Sv
Ekman upwelling+eddy return flow, $q_{SO}(t_o)$	7.4 Sv	19.5 Sv	19.5 Sv
diapycnal upwelling, $q_v(t_o)$	5.6 Sv	4.2 Sv	4.2 Sv
upper ocean depth in low latitudes, $h(t_o)$	362 m	487 m	487 m
temperature, $T_N(t_o)$, $T_S(t_o)$ and $T_{deep}(t_o)$	5^oC	5^oC	5^oC
temperature, $T_{ml}(t_o)$	25^oC	25^oC	25^oC
temperature, $T_{therm}(t_o)$	10.7^oC	13.2^oC	6.7^oC
heat uptake, $N_S(t_o)$	0 W	0 W	0 W
heat uptake, $N_N(t_o)$	-3×10^{14} W	-8×10^{14} W	-1.6×10^{14} W
heat uptake, $N_{ml}(t_o)$	3×10^{14} W	8×10^{14} W	1.6×10^{14} W
carbon, $DIC_N(t_o)$, $DIC_S(t_o)$ and $DIC_{deep}(t_o)$	2140 μmol kg^{-1}	2140 μmol kg^{-1}	2140 μmol kg^{-1}
carbon, $DIC_{ml}(t_o)$,	1945 μmol kg^{-1}	1945 μmol kg^{-1}	1945 μmol kg^{-1}
carbon, $DIC_{therm}(t_o)$,	2085 μmol kg^{-1}	2060 μmol kg^{-1}	2124 μmol kg^{-1}
carbon uptake, $F_S(t_o)$	0 mol s^{-1}	0 mol s^{-1}	0 mol s^{-1}
carbon uptake, $F_N(t_o)$	7.4×10^5 mol s^{-1}	2×10^6 mol s^{-1}	3.9×10^5 mol s^{-1}
carbon uptake, $F_{ml}(t_o)$	-7.4×10^5 mol s^{-1}	-2×10^6 mol s^{-1}	-3.9×10^5 mol s^{-1}

LIST OF FIGURES

Fig. 1. Idealised atmosphere-ocean models: (a) the 1D box model with three layers, a slab atmosphere (grey), ocean mixed layer (pale blue) and ocean interior (dark blue); and (b) the box model with overturning circulation including a slab atmosphere (grey), an upper layer of light water consisting of a thermocline layer (light blue) and a surface mixed layer (pale blue) in the low latitudes, and two upper layers at southern and northern high latitudes and a lower layer of dense water (darker shades of blue). The upper layer of light water in the low latitudes has a thickness of $h(t) = h_{therm}(t) + h_{ml}$. Heat and carbon fluxes into the atmosphere and from the atmosphere into the ocean driven by carbon emissions are denoted by red and blue arrows, respectively, while the volume transports between the different ocean layers are denoted by black arrows. The isolation fraction δ represents the proportion of mode waters formed in the Southern Ocean, which are shielded from the atmosphere in the low latitudes. 40

Fig. 2. The evolution of the volume transports and the thickness of the light waters from the pre-industrial state in the box model with overturning forced by emissions, from selected ensemble members with $\tau_{wind} = 0.05$, 0.1 and 0.15 N m^{-2}, corresponding to an overturning at the pre-industrial of $q_{NA}(to) = 13$, 24 and 35 Sv, respectively, and a fraction of isolation $\delta = 50\%$: (a) the volume rate of transformation of light water into dense water at the northern high latitudes, q_{NA} (Sv), equivalent to the strength of meridional overturning; (b) the volume rate of transformation of the dense water into light waters in the southern high latitudes, q_{so} (Sv), equivalent to the residual circulation; (c) the volume rate of transformation of dense waters into light waters associated with diapycnal mixing in low latitudes, q_v (Sv); and (d) the thickness of light waters, h (m). The thin black dotted line denotes the cessation of the emissions. 41

Fig. 3. Carbon and heat budgets in the 1D box model from an ensemble member with a mixed-layer thickness of $h_{ml} = 100$ m and a ventilation timescale of $\tau_{vent} = 1000$ y (left panels), and in the box model with overturning from an ensemble member with a Southern Ocean wind stress of $\tau_{wind} = 0.1$ N m^{-2}, corresponding to an overturning at the pre-industrial of $q_{NA}(t_o) = 24$ Sv, and a fraction of isolation of $\delta = 50\%$ (right panels): (a) and (c) the cumulative carbon emissions, $I_{em}(t)$ in PgC, and the changes in the atmosphere and ocean carbon inventories relative to the pre-industrial, $\Delta I_{atm}(t)$ and $\Delta I_{ocean}(t)$ in PgC, respectively, along with the carbon contribution to the TCRE, $R(t)/I_{em}(t)$ in W m^{-2} (1000PgC)$^{-1}$; and (b) and (d) the radiative forcing, $R(t)$ in W m^{-2}, the radiative response, $\lambda \Delta T(t)$ in W m^{-2}, and the net heat uptake, $N(t)$ in W m^{-2}, along with the thermal contribution to the TCRE, $\Delta T(t)/R(t)$ in K (W m^{-2})$^{-1}$. The thin black dotted line denotes the cessation of the emissions. 42

Fig. 4. Sensitivity to the mixed-layer thickness from selected ensemble members with a ventilation timescale of $\tau_{vent} = 500$ y and mixed-layer thickness of $h_{ml} = 50$, 100 and 300 m (left panels) and to the rate of the ventilation of the ocean interior from selected ensemble members with a mixed-layer thickness of $h_{ml} = 100$ m and a ventilation timescale of $\tau_{vent} = 100$, 500, and 1000 y (right panels) in the 1D box model: (a) and (d) the TCRE, $\Delta T(t)/I_{em}(t)$ in K (1000PgC)$^{-1}$; (b) and (e) carbon contribution to the TCRE, $R(t)/I_{em}(t)$ in W m^{-2} (1000PgC)$^{-1}$; and (c) and (f) thermal contribution to the TCRE, $\Delta T(t)/R(t)$ in K (W m^{-2})$^{-1}$. The thin black dotted line denotes the cessation of the emissions. 43

Fig. 5. Sensitivity to the mixed-layer thickness and the ventilation timescale in the 1D box model at year 10 (left panels), at year 100 (middle panels) and at year 500 (right panels): (a) the TCRE, $\Delta T(t)/I_{em}(t)$; (b) carbon contribution to the TCRE, $R(t)/I_{em}(t)$; and (c) thermal contribution to the TCRE, $\Delta T(t)/R(t)$. The estimates are based on the ensemble with variations in both the mixed-layer thickness and the ventilation timescale. 44

Fig. 6. Sensitivity to the strength of the overturning circulation from selected ensemble members with a fraction of isolation $\delta = 50\%$ and a Southern Ocean wind stress $\tau_{wind} = 0.05$, 0.1 and 0.15 N m^{-2} corresponding to overturning at the pre-industrial of $q_{NA}(t_o) = 13$, 24 and 35 Sv, respectively (left panels), and to the fraction of isolation from selected ensemble members with a Southern Ocean wind stress $\tau_{wind} = 0.1$ N m^{-2} corresponding to an overturning at the pre-industrial of $q_{NA}(t_o) = 24$ Sv and a fraction of isolation $\delta = 10$, 50 and 90% (right panels) in the box model with overturning: (a) and (d) the TCRE, $\Delta T(t)/I_{em}(t)$ in K (1000PgC)$^{-1}$; (b) and (e) carbon contribution to the TCRE, $R(t)/I_{em}(t)$ in W m^{-2} (1000PgC)$^{-1}$; and (c) and (f) thermal contribution to the TCRE, $\Delta T(t)/R(t)$ in K (W m^{-2})$^{-1}$. The thin black dotted line denotes the cessation of the emissions. 45

Fig. 7. Sensitivity to the overturning strength, q_{NA}, and the fraction of isolation, δ, in the box model with overturning at year 10 (left panels), at year 100 (middle panels) and at year 500 (right panels): (a) the TCRE, $\Delta T(t)/I_{em}(t)$; (b) carbon contribution to the TCRE, $R(t)/I_{em}(t)$; and (c) thermal contribution to the TCRE, $\Delta T(t)/R(t)$. A large isolation fraction implies more subduction in the Southern Ocean and less atmosphere-ocean interaction in the low latitudes. The estimates are based on the ensemble with variations in both the wind stress and the fraction of isolation. 46

Fig. 8. The variability of the TCRE (black lines) and its partition into a carbon contribution, $R(t)/I_{em}(t)$ (blue lines), and a thermal contribution, $\Delta T(t)/R(t)$ (red lines). The variability in the 1D box model driven by (a) the combined changes in the mixed-layer thickness and the ventilation timescale; and separately by (b) changes in the mixed-layer thickness and (c) changes in the ventilation timescale. The variability in the box model with overturning driven by (d) the combined changes in the strength of the overturning circulation and the isolation fraction; and separately by (e) changes in the strength of the overturning and (f) changes in the isolation fraction. The variability is represented by the coefficient of variation, defined by the standard deviation divided by the mean for the model ensemble for each set of ventilation experiment (Table 1). The *x* axes denoting years is presented in a logarithmic scale. The thin black dotted line denotes the cessation of the emissions. 47

Fig. 9. The variability of the TCRE (black lines) and its partition into a carbon contribution, $R(t)/I_{em}(t)$ (blue lines), and a thermal contribution, $\Delta T(t)/R(t)$ (red lines) driven by different aspects of the ocean ventilation for different carbon emission rate and timing of cessation of emissions: (a) the mixed-layer thickness; (b) the ventilation timescale; (c) the strength of the overturning circulation; and (d) the isolation fraction. The variability is represented by the coefficient of variation, defined by the standard deviation divided by the mean for the model ensemble for each set of ventilation experiment (Table 1). The *x* axes denoting years is presented in a logarithmic scale. The thin black dotted line denotes the cessation of the emissions. 48

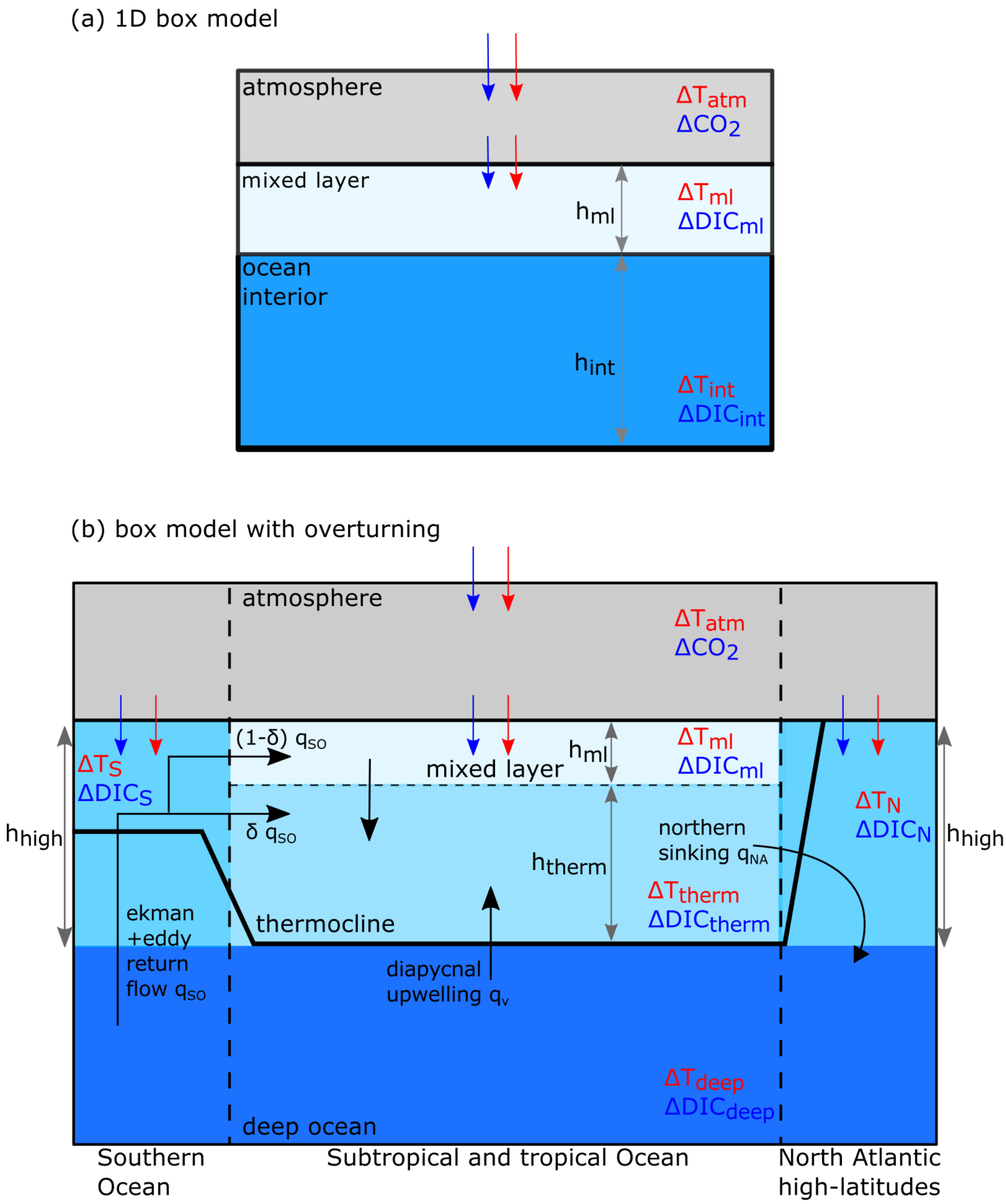

FIG. 1. Idealised atmosphere-ocean models: (a) the 1D box model with three layers, a slab atmosphere (grey), ocean mixed layer (pale blue) and ocean interior (dark blue); and (b) the box model with overturning circulation including a slab atmosphere (grey), an upper layer of light water consisting of a thermocline layer (light blue) and a surface mixed layer (pale blue) in the low latitudes, and two upper layers at southern and northern high latitudes and a lower layer of dense water (darker shades of blue). The upper layer of light water in the low latitudes has a thickness of $h(t) = h_{therm}(t) + h_{ml}$. Heat and carbon fluxes into the atmosphere and from the atmosphere into the ocean driven by carbon emissions are denoted by red and blue arrows, respectively, while the volume transports between the different ocean layers are denoted by black arrows. The isolation fraction δ represents the proportion of mode waters formed in the Southern Ocean, which are shielded from the atmosphere in the low latitudes.

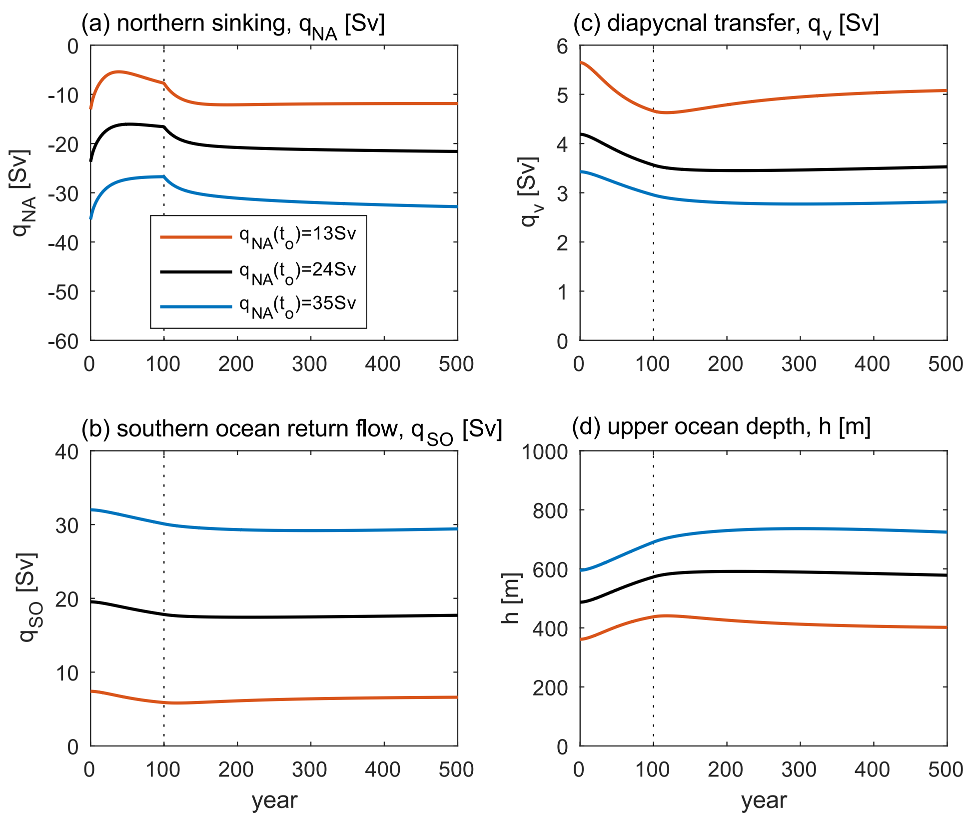

FIG. 2. The evolution of the volume transports and the thickness of the light waters from the pre-industrial state in the box model with overturning forced by emissions, from selected ensemble members with $\tau_{wind} = 0.05$, 0.1 and 0.15 N m^{-2}, corresponding to an overturning at the pre-industrial of $q_{NA}(to) = 13$, 24 and 35 Sv, respectively, and a fraction of isolation $\delta = 50\%$: (a) the volume rate of transformation of light water into dense water at the northern high latitudes, q_{NA} (Sv), equivalent to the strength of meridional overturning; (b) the volume rate of transformation of the dense water into light waters in the southern high latitudes, q_{so} (Sv), equivalent to the residual circulation; (c) the volume rate of transformation of dense waters into light waters associated with diapycnal mixing in low latitudes, q_v (Sv); and (d) the thickness of light waters, h (m). The thin black dotted line denotes the cessation of the emissions.

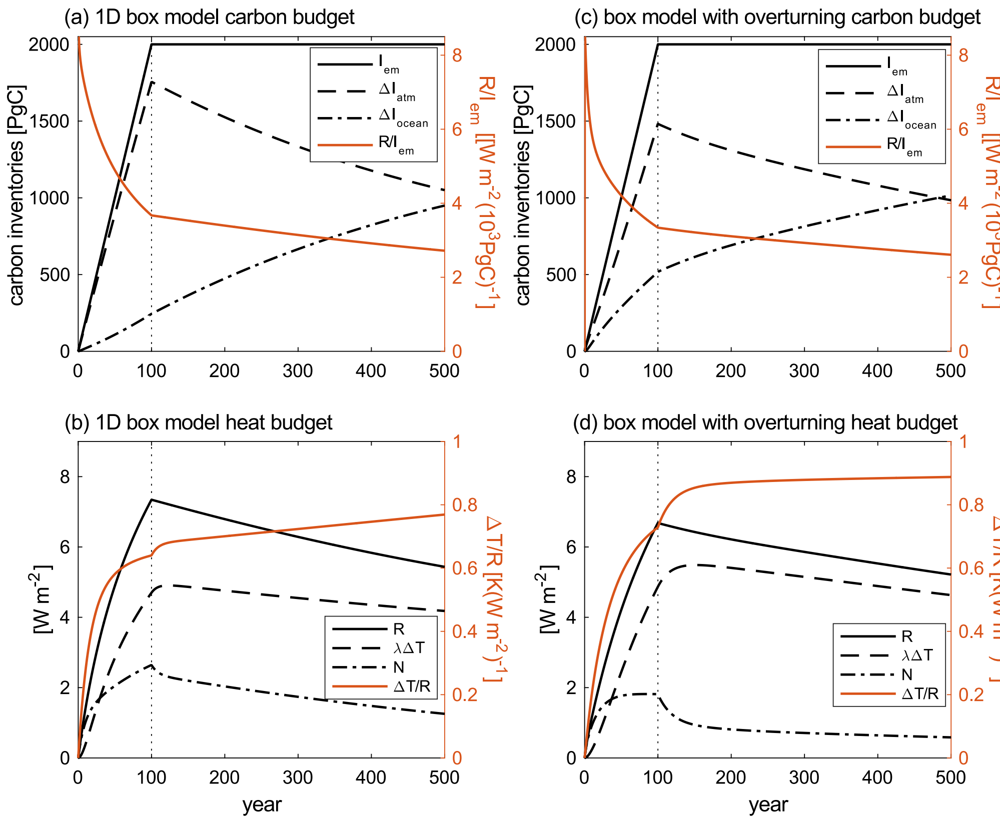

FIG. 3. Carbon and heat budgets in the 1D box model from an ensemble member with a mixed-layer thickness of $h_{ml} = 100$ m and a ventilation timescale of $\tau_{vent} = 1000$ y (left panels), and in the box model with overturning from an ensemble member with a Southern Ocean wind stress of $\tau_{wind} = 0.1$ N m^{-2}, corresponding to an overturning at the pre-industrial of $q_{NA}(t_o) = 24$ Sv, and a fraction of isolation of $\delta = 50\%$ (right panels): (a) and (c) the cumulative carbon emissions, $I_{em}(t)$ in PgC, and the changes in the atmosphere and ocean carbon inventories relative to the pre-industrial, $\Delta I_{atm}(t)$ and $\Delta I_{ocean}(t)$ in PgC, respectively, along with the carbon contribution to the TCRE, $R(t)/I_{em}(t)$ in W m^{-2} (1000PgC)$^{-1}$; and (b) and (d) the radiative forcing, $R(t)$ in W m^{-2}, the radiative response, $\lambda \Delta T(t)$ in W m^{-2}, and the net heat uptake, $N(t)$ in W m^{-2}, along with the thermal contribution to the TCRE, $\Delta T(t)/R(t)$ in K (W m^{-2})$^{-1}$. The thin black dotted line denotes the cessation of the emissions.

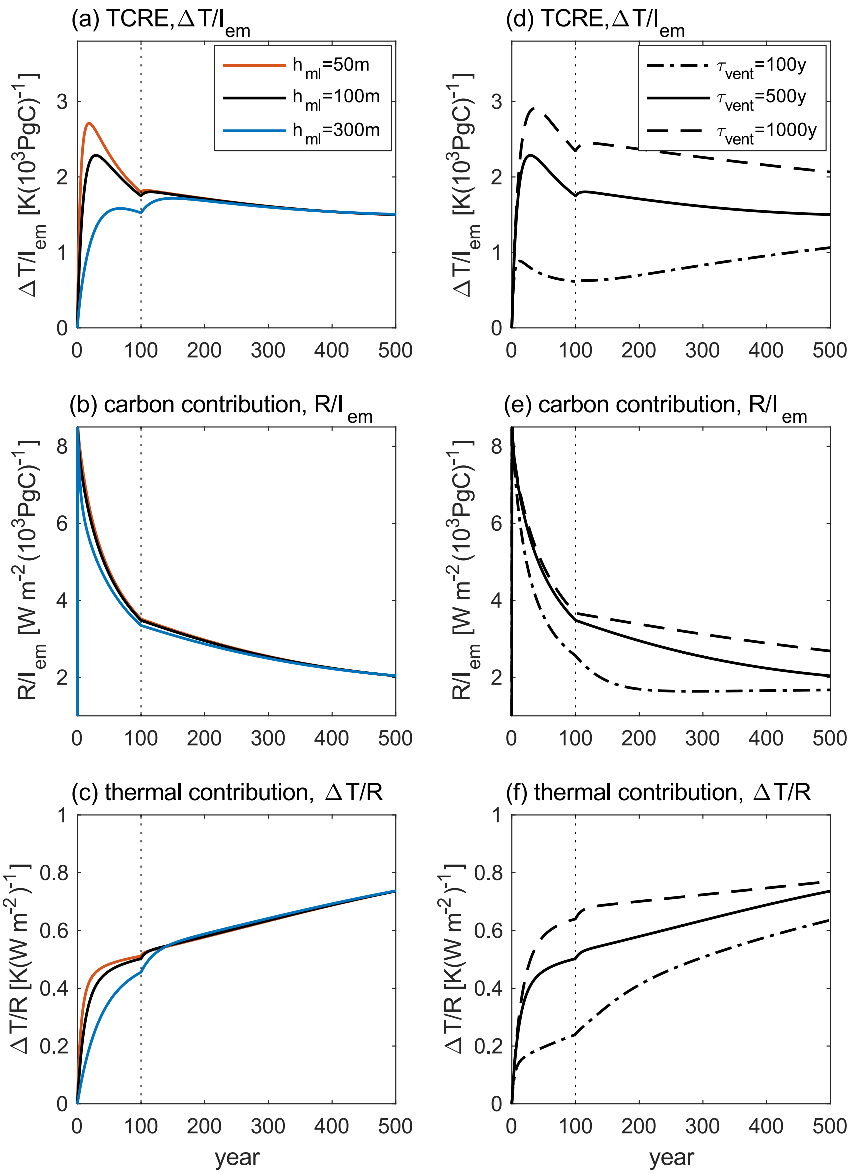

856 FIG. 4. Sensitivity to the mixed-layer thickness from selected ensemble members with a ventilation timescale of $\tau_{vent} = 500$ y and mixed-layer thickness of $h_{ml} = 50$, 100 and 300 m (left panels) and to the rate of the ventilation of the ocean interior from selected ensemble members with a mixed-layer thickness of $h_{ml} = 100$ m and a ventilation timescale of $\tau_{vent} = 100$, 500, and 1000 y (right panels) in the 1D box model: (a) and (d) the TCRE, $\Delta T(t)/I_{em}(t)$ in K (1000PgC)$^{-1}$; (b) and (e) carbon contribution to the TCRE, $R(t)/I_{em}(t)$ in W m^{-2} (1000PgC)$^{-1}$; and (c) and (f) thermal contribution to the TCRE, $\Delta T(t)/R(t)$ in K (W m^{-2})$^{-1}$. The thin black dotted line denotes the cessation of the emissions.

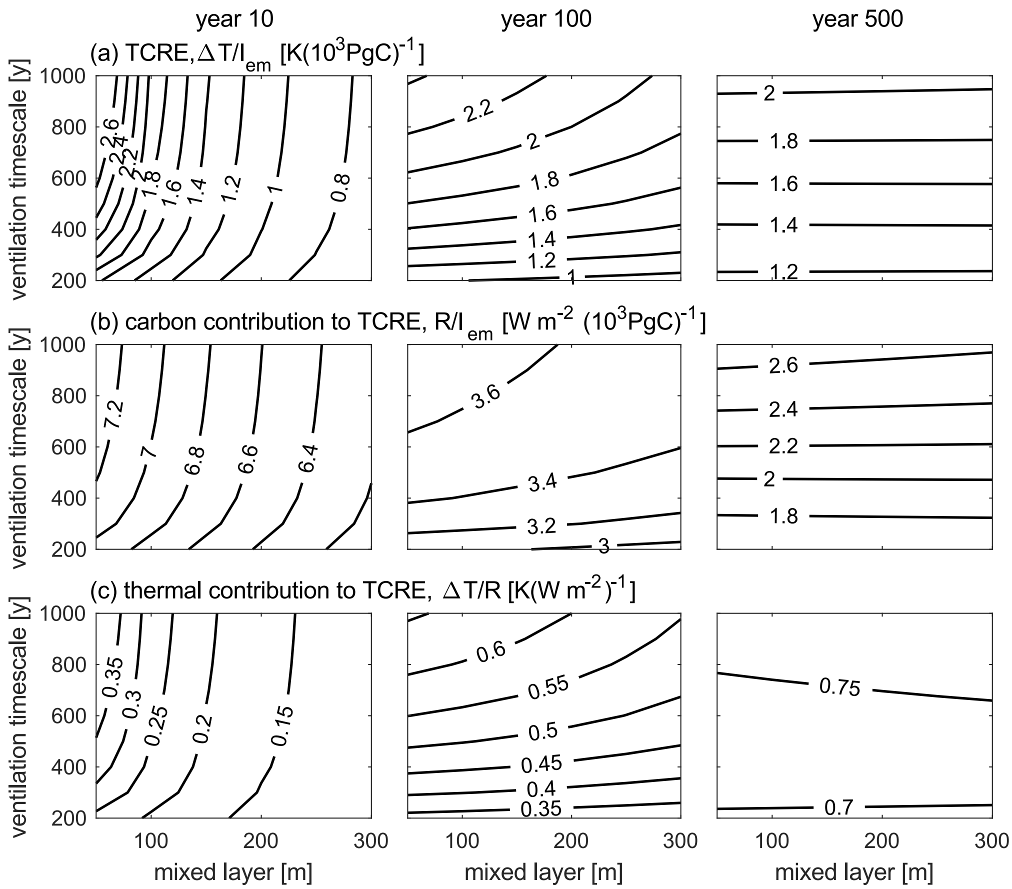

FIG. 5. Sensitivity to the mixed-layer thickness and the ventilation timescale in the 1D box model at year 10 (left panels), at year 100 (middle panels) and at year 500 (right panels): (a) the TCRE, $\Delta T(t)/I_{em}(t)$; (b) carbon contribution to the TCRE, $R(t)/I_{em}(t)$; and (c) thermal contribution to the TCRE, $\Delta T(t)/R(t)$. The estimates are based on the ensemble with variations in both the mixed-layer thickness and the ventilation timescale.

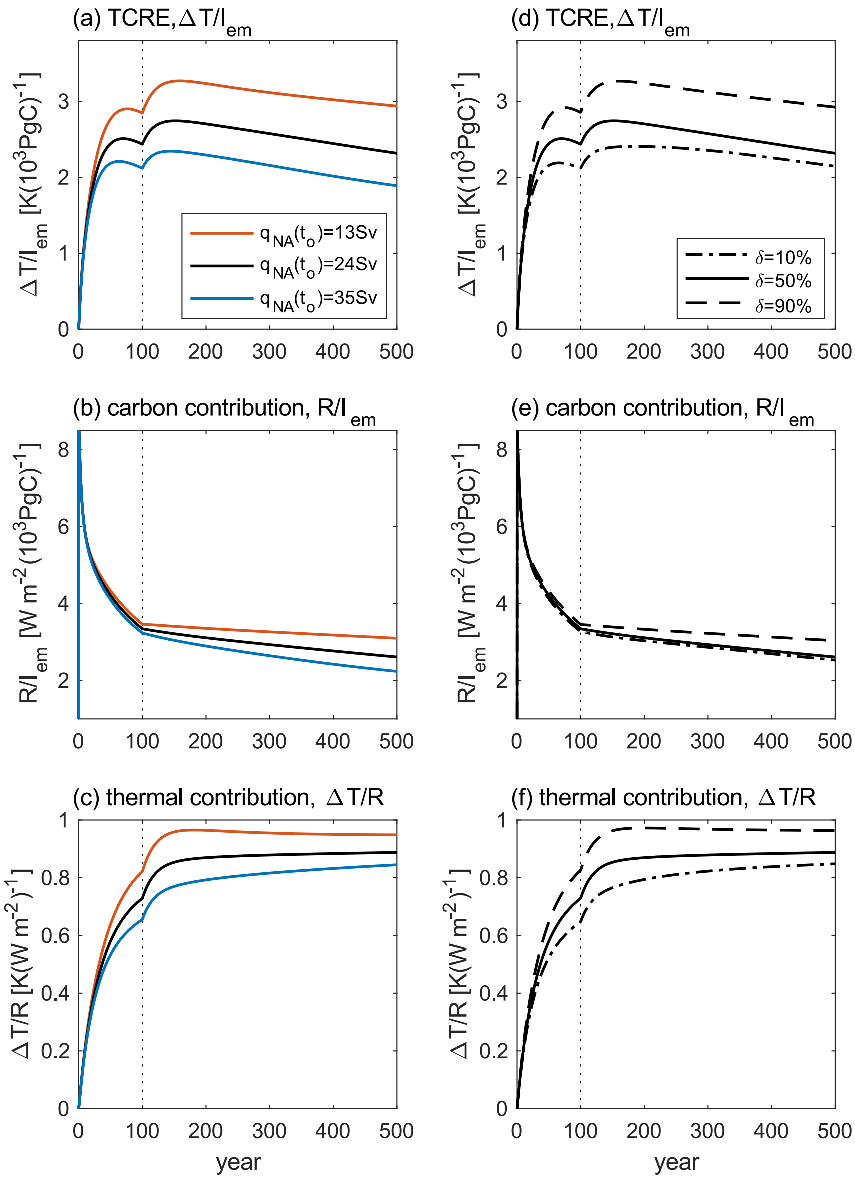

FIG. 6. Sensitivity to the strength of the overturning circulation from selected ensemble members with a fraction of isolation $\delta = 50\%$ and a Southern Ocean wind stress $\tau_{wind} = 0.05$, 0.1 and 0.15 N m^{-2} corresponding to an overturning at the pre-industrial of $q_{NA}(t_o) = 13$, 24 and 35 Sv, respectively (left panels), and to the fraction of isolation from selected ensemble members with a Southern Ocean wind stress $\tau_{wind} = 0.1$ N m^{-2} corresponding to an overturning at the pre-industrial of $q_{NA}(t_o) = 24$ Sv and a fraction of isolation $\delta = 10$, 50 and 90% (right panels) in the box model with overturning: (a) and (d) the TCRE, $\Delta T(t)/I_{em}(t)$ in K (1000PgC)$^{-1}$; (b) and (e) carbon contribution to the TCRE, $R(t)/I_{em}(t)$ in W m^{-2} (1000PgC)$^{-1}$; and (c) and (f) thermal contribution to the TCRE, $\Delta T(t)/R(t)$ in K (W m^{-2})$^{-1}$. The thin black dotted line denotes the cessation of the emissions.

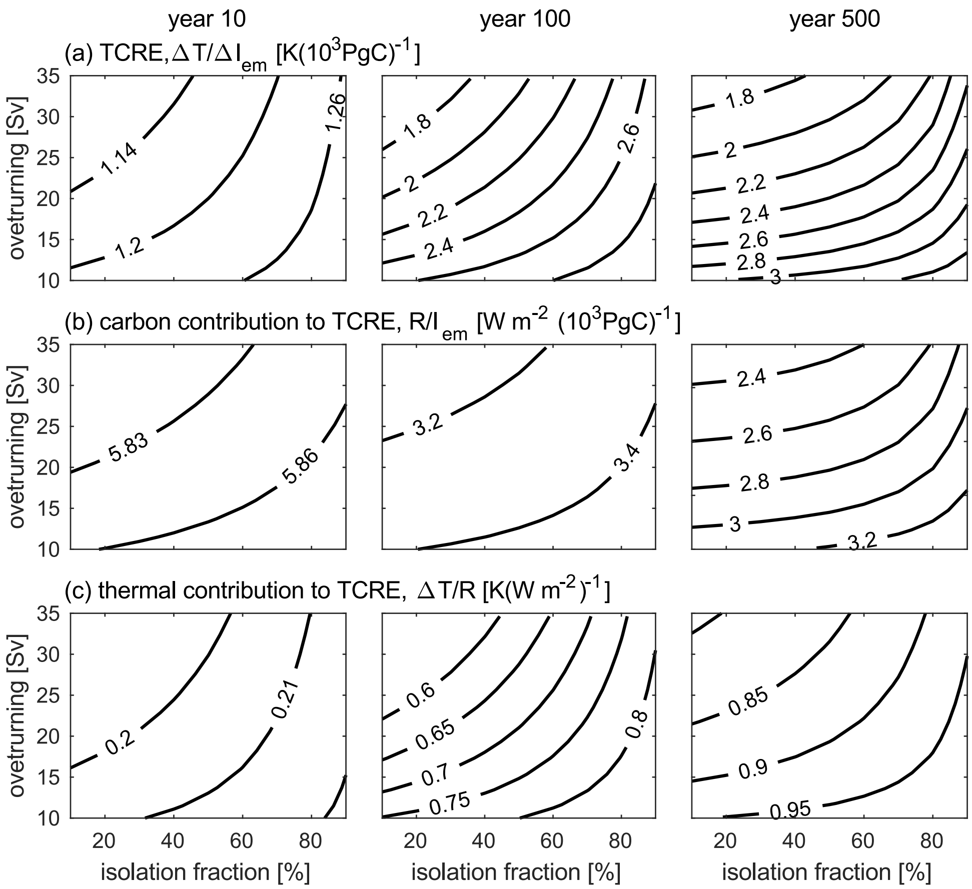

FIG. 7. Sensitivity to the overturning strength, q_{NA}, and the fraction of isolation, δ, in the box model with overturning at year 10 (left panels), at year 100 (middle panels) and at year 500 (right panels): (a) the TCRE, $\Delta T(t)/I_{em}(t)$; (b) carbon contribution to the TCRE, $R(t)/I_{em}(t)$; and (c) thermal contribution to the TCRE, $\Delta T(t)/R(t)$. A large isolation fraction implies more subduction in the Southern Ocean and less atmosphere-ocean interaction in the low latitudes. The estimates are based on the ensemble with variations in both the wind stress and the fraction of isolation.

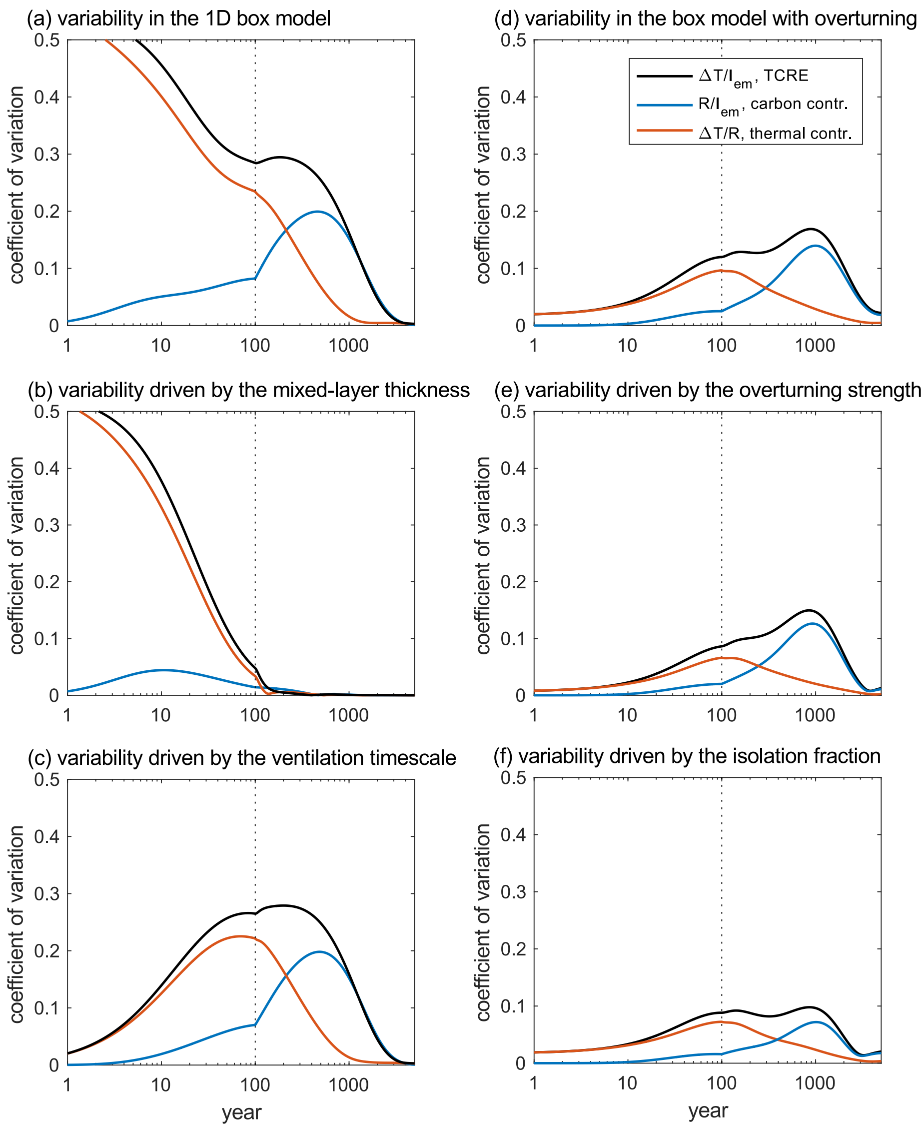

FIG. 8. The variability of the TCRE (black lines) and its partition into a carbon contribution, $R(t)/I_{em}(t)$ (blue lines), and a thermal contribution, $\Delta T(t)/R(t)$ (red lines). The variability in the 1D box model driven by (a) the combined changes in the mixed-layer thickness and the ventilation timescale; and separately by (b) changes in the mixed-layer thickness and (c) changes in the ventilation timescale. The variability in the box model with overturning driven by (d) the combined changes in the strength of the overturning circulation and the isolation fraction; and separately by (e) changes in the strength of the overturning and (f) changes in the isolation fraction. The variability is represented by the coefficient of variation, defined by the standard deviation divided by the mean for the model ensemble for each set of ventilation experiment (Table 1). The x axes denoting years is presented in a logarithmic scale. The thin black dotted line denotes the cessation of the emissions.

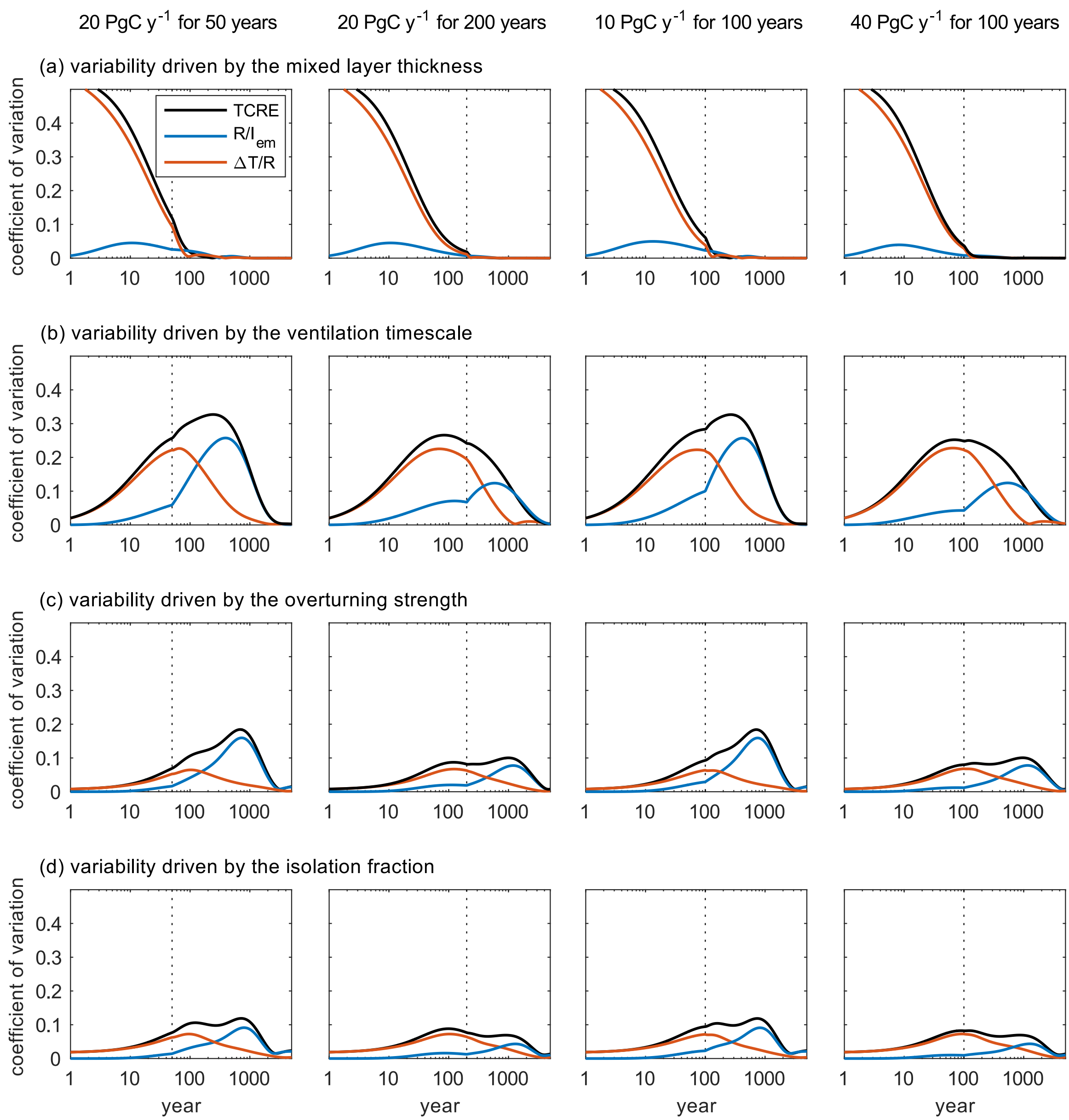

891 FIG. 9. The variability of the TCRE (black lines) and its partition into a carbon contribution, $R(t)/I_{em}(t)$ (blue lines), and a thermal contribution, $\Delta T(t)/R(t)$ (red lines) driven by different aspects of the ocean ventilation for different carbon emission rate and timing of cessation of emissions: (a) the mixed-layer thickness; (b) the ventilation timescale; (c) the strength of the overturning circulation; and (d) the isolation fraction. The variability is represented by the coefficient of variation, defined by the standard deviation divided by the mean for the model ensemble for each set of ventilation experiment (Table 1). The x axes denoting years is presented in a logarithmic scale. The thin black dotted line denotes the cessation of the emissions.